الجمهورية الديمقراطية الشعبية الجزائرية

République Algérienne Démocratique et Populaire

Ministère de l'Enseignement Supérieur et de la Recherche Scientifique
Ecole Supérieure des Sciences Appliquées d'Alger

وزارة التعليم العالي والبحث العلمي
المدرسة العليا في العلوم التطبيقية بالجزائر

Département du second cycle

Mémoire de Fin d'Etudes

En vue de l'obtention du diplôme d'ingéniorat d'état

Filière : **Electrotechnique**

Spécialité : **Traction électrique**

Thème :

Induction Machine Faults Diagnosis : Ball Bearing Consideration

Présenté par : Bayou Nada

Encadré par : Deboucha abdelhakim
Co-encadré par : Ounnas Bedreddine

Soutenu publiquement, le : 20/09/2021,

Devant le Jury composé de :

Dr Hamache Amar	Président
Dr Deboucha Abdelhakim	Encadreur
Dr Bensenouci Ahmed	Examinateur

Binôme N° : 13/PFE. / 2021

Abstract

Induction machine (IM) are nowadays widely used in most industry applications systems, due to their simple construction, high reliability, and the availability of power converters using efficient control strategies. IM are subjected to some undesirable stresses during their operating lifetime, causing them to a number of failures. Ball bearing defects shares considerable percentage of the machine failures, these defects may be due to manufacturing errors and/or operating conditions. With the industrial growth and advancement, it has become necessary to monitor the condition of the machine while operating. Hence, condition monitoring of bearings has been considered to be an essential and an integral part of any modern manufacturing facility.

In this study, simulation base of an induction machine and its bearing when faulty/healthy is addressed. In order to detect the bearing faults, Fast Fourier Transform (FFT) is proposed to analyze the spectral of the stator's current.

This work presents a model of the machine as well as an analytical model for the ball bearing which are simulated using MATLAB software. Ball bearing defect could be either inner or outer race faults, hence, both deficiencies were modeled and associated with the load torque parameter of the IM.

Simulation results show that the time domain analysis indicates the existence of a bearing defect, on the other hand the spectral analysis shows in which part of the bearing the defect is found.

Keywords: Induction machine, ball bearing, faults detection, FFT, spectral analysis.

Résumé

Les machines à induction (IM) sont aujourd'hui largement utilisées dans tous les types de systèmes d'applications industrielles en raison de leur construction simple, de leur haute fiabilité et de la disponibilité de convertisseurs de puissance utilisant des stratégies de contrôle efficaces, les IM sont soumises à des contraintes indésirables au cours de leur durée de vie, provoquant des échecs. Les défauts des roulements à billes sont partagés à non négligeable pourcentage des pannes de la machine, ces défauts peuvent être dus à des erreurs de fabrication et aux conditions de fonctionnement. Avec la croissance industrielle, il est devenu nécessaire de surveiller l'état de la machine. Par conséquent, la surveillance de l'état des roulements a été considérée comme une partie essentielle et intégrale de toute installation de fabrication moderne.

Cette étude porte sur l'application de l'analyse spectrale du courant moteur pour la détection des dommages aux roulements à billes dans les machines à induction en utilisant une méthode de traitement du signal qui est la transformée de Fourier rapide (FFT) qui montre toute fréquence anormale liée au défaut dans le spectre du signal.

Ce travail présente un modèle de la machine ainsi qu'un modèle analytique du roulement à billes qui sont simulés à l'aide du logiciel MATLAB, dans un cas sain et avec des défauts dans le chemin intérieur et le chemin extérieur du roulement à billes. La présence de défauts sur les chemins de roulement à billes génère des changements notables dans le spectre de courant statorique.

Les résultats de la simulation montrent que l'analyse dans le domaine temporel indique l'existence d'un défaut de roulement, d'autre part l'analyse spectrale montre localise roulement le défaut du roulement.

الملخص

تُستخدم الآلات اللاتزامنية (lM) على نطاق واسع في جميع أنواع أنظمة التطبيقات الصناعية نظرًا لبنيتها البسيطة وموثوقيتها العالية وتوفر محولات الطاقة باستخدام استراتيجيات التحكم الفعالة . تتعرض الآلة اللاتزامنية(IM) لضغوط غير مرغوب فيها خلال عمرها الافتراضي ، مما يتسبب في حدوث أعطال. تعتبر عيوب المدحرجات الكروية السبب الرئيسي لفشل الآلة ، ويمكن أن تكون هذه العيوب ناتجة عن أخطاء التصنيع وظروف التشغيل. مع النمو الصناعي، أصبح من الضروري مراقبة حالة الآلة. لذلك ، تم اعتبار مراقبة حالة المدحرجة جزءًا أساسيًا لا يتجزأ من أي منشأة تصنيع حديثة.

تركز هذه الدراسة على تطبيق التحليل الطيفي للتيار للكشف عن الأضرار التي لحقت بالمدحرجات الكروية في الآلات اللاتزامنية باستخدام طريقة معالجة الإشارة وهي FFT والتي تظهر أي تردد غير طبيعي مرتبط بالخلل في طيف الإشارة الاساسي.

يقدم هذا العمل نموذجًا للآلة بالإضافة إلى نموذج تحليلي للمدحرجات الكروية الذي تمت محاكاته باستخدام برنامج MATLAB , في الحالة السليمة مع وجود عيوب في الحلقة الداخلية أو الحلقة الخارجية للمدحرجات الكروية. يتسبب وجود عيوب في المدحرجة تغيرات ملحوظة في الطيف الحالي للجزء الثابت.

تظهر نتيجة المحاكاة أن تحليل المجال الزمني يشير إلى وجود عطل في المدحرجة و من ناحية أخرى ، يُظهر التحليل الطيفي أي جزء من المدحرجة يوجد فيه العطل .

الكلمات المفتاحية: الآلة اللاتزامنية، المدحرجات الكروية ،عطب الحلقة الداخلية ،عطب الحلقة الخارجية ،FFT.

Acknowledgements

Praises be to Allah for providing me the time, good health and strength to work in completing this study

First and foremost, I would like to sincerely thank my Advisor **Dr. DEBOUCHA Abdelhakim** for his guidance, understanding, patience and most importantly, he has provided positive encouragement and a warm spirit to finish this thesis. It has been a great pleasure and honor to have him as my supervisor

My deepest gratitude goes to all of my family members. It would not be possible to write this thesis without the support from them. I would like to present my gratitude to my parents for their warm encouragement, their invaluable sacrifices and their great confidence.

I would particularly like to thank **Mr. Amar HAMACHE** who did as an honor of chairing this jury as well as **Mr. Ahmed BENSNOUCI**, for accepting the examination of this work.

Finally, my heartfelt thanks go to all my lecturers for their help and support during my studies.

Dedication

In the name of Allah, the Most Gracious and the Most Merciful. All praises to Allah and His blessing for the completion of this thesis. I thank God for all the opportunities, trials and strength that have been showered on me to finish writing the thesis.

I dedicate this work,

To my father and my mother, for their motivation, prayers and their sincere help during my studies.

To my brothers AMINE and ABDELHAK and my sisters AMIRA and AMEL who are always supported and encouraged me.

To my friend Moh for his help and encouragement, to my best friends Racha, Rosa, Fethia and Karima with whom i spent unforgettable moments, and to all my friends from ESSA ALGIERS and ENP.

To all who support me and believe in me, and all my family and who give me love and liveliness.

NADA

Table of Contents

List of Figures

LIST OF SYMBOLS

N_s	Number of turns in the stator winding
n_b	Number of rotor bars
k	Integer number
p	Number of pair poles
θ_r	The rotor angular position [rad]
r	Mean diameter of the machine
l	Length of the slots in the stator.
J	Moment of Inertia [kg.m^2]
T_L	Load torque [N.m]
T_e	Electromagnetic torque [N.m]
W_{co}	Co-energy
ϕ_s	The stator flux vector [Wb]
ϕ_r	The rotor flux vector [Wb]
L_{am}	The magnetizing inductance of the phase “a” [H]
L_{sl}	Leakage inductance [H]
L_s	Stator inductance [H]
L_{sr}	The mutual inductance between the rotor loop and the stator winding [H]
L_b	Rotor bar inductance [H]
L_e	Rotor end ring inductance [H]
L_r	Rotor inductance [H]
M_s	Mutual Stator inductance
r_s	Stator winding resistance [Ω]
R_s	Total Stator resistance [Ω]
R_r	Total Rotor resistance [Ω]
R_{bk}	Rotor bar resistance [Ω]
R_e	End ring resistance [Ω]
V_s	Stator voltage vector [V]

V_{as}	Stator voltage vector of phase “a” [V]
V_{bs}	Stator voltage vector of phase “b” [V]
V_{cs}	Stator voltage vector of phase “c” [V]
V_{rk}	Rotor loop voltage [V]
V_{re}	Rotor end ring voltage [V]
I_s	Stator current vector [A]
I_{as}	Stator current vector of phase “a” [A]
I_{bs}	Stator current vector of phase “b” [A]
I_{cs}	Stator current vector of phase “c” [A]
I_{rk}	Rotor loop current [A]
I_{re}	Rotor end ring current [A]
d	Ball diameter [m]
D	pitch diameter of bearing [m]
c	damping factor [N s/m]
C_r	Radial clearance [m]
F	Hertzian contact force [N]
F_X, F_Y,F_{XD}, F_{YD}	Components of restoring forces in X and Y directions [N]
H_D	Height of defect [m]
K,K_p,K_i,K_o	Load–deformation factor [N/m$^{3/2}$]
M	Mass of the rotor [kg]
n	Load–deflection exponent
W	Radial load (N)
x, y	Deflections along X and Y axes (m)
Z	Number of balls
δ_r	Radial deflection (m)
δ^*	Dimensionless contact deformation
Σp	Curvature sum
ϕ	Length of defect in [deg].
θ_i	Initial position of the defect [deg]
w	Shaft speed [rad/s]
w_c	Cage speed [rad/s]

f_{am_be}	Characteristic frequency of the ball fault seen on the current [Hz]
f_{am_ex}	Characteristic frequency of the outer raceway fault seen on the current [Hz]
f_{am_in}	Characteristic frequency of the inner raceway seen on the current [Hz]
f_{bi}	Characteristic frequency of the ball fault [Hz]
f_{in}	Characteristic frequency of the inner raceway fault [Hz]
f_r	Mechanical rotational frequency of rotor [Hz].
f_s	Stator supply frequency [Hz].
A	Permeance of the air gap

CHAPTER I

INTRODUCTION

I.1 Background

The industrial world has become increasingly using efficient and complex machines and installations. Rotating machine is an essential element in the industrial environment where the bearing plays a major role in making these machines rotate (S. KASS, 2019). Among these machine, induction machine (IM) are nowadays widely used in all types of industry applications systems including aviation systems, electric rail traction, cooling of power plants or industrial production lines due to their simple construction, high reliability, and the availability of power converters using efficient control strategies.

Squirrel cage induction machine is considered to be the most robust of its generation and the least expensive to manufacture. IM is often used in industrial applications, not only at low-risk environment (pumps, conveyors, machine tools and compressors) but also in dangerous and aggressive places such as gas factories, petrochemicals plants ... etc.

The use of electric machines in complex industrial systems has been accompanied by a greater demand due to their availability and reliability. However, these machines are subjected to failures either electrical failures (stator /rotor faults) or mechanical failures (bearing faults, rotor eccentricity). According to statistics given in (T. Lindh, 2003), 40% of breakdowns in an industrial installation are linked to the electrical system, of which 24% are due to rotating electrical machines, where bearing faults are the most frequent faults in electric motors 41% according to IEEE motor reliability study for large motors above 200 HP, followed by stator 37% and rotor faults 10% as shown in figure I.1 (M. Blödt, 2008). Therefore, a permanent condition monitoring of the electrical drive can further increase the productivity, reliability, and safety of the entire installation.

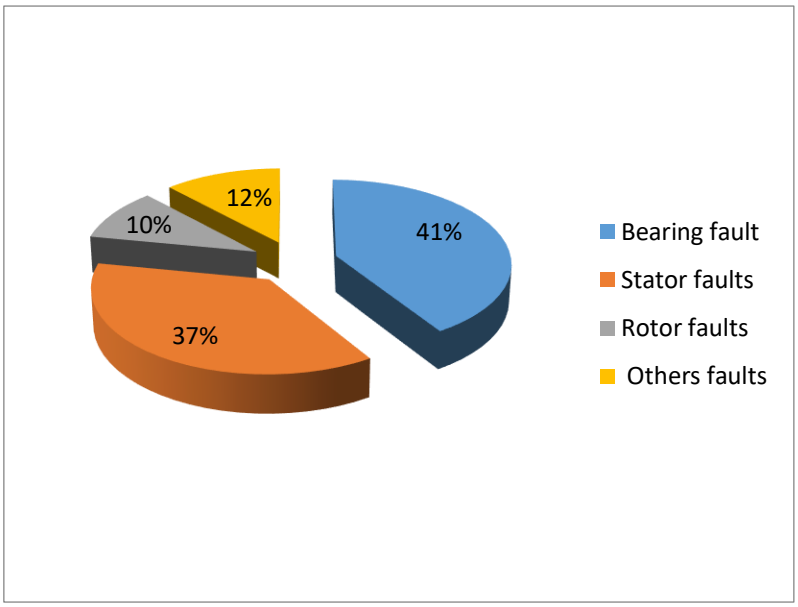

Figure I.1: Different failure modes of the induction motor.

Rolling element bearings find widespread domestic and industrial applications. Proper functioning of these appliances depends, to a great extent, on the smooth and quiet running of the bearings. In industrial applications, these bearings are considered as critical mechanical components and a defect in such a bearing, unless detected in time, causes malfunction and may even lead to catastrophic failure of the machinery. Defects in bearings may arise during use or during the manufacturing process (N. Tandon, et al, 1999). Their failure is one of the most common problems that occur with a high probability up to 90% in small machines (C. Bianchini, et al, 2011). Therefore, detection of these defects is important for condition monitoring as well as quality inspection of the bearings. Different methods are used for detection and diagnosis of bearing defects; they may be broadly classified as vibration and acoustic measurements, temperature measurements and wear debris analysis. Among these, vibration measurements are the most widely used (N. Tandon, et al, 1999). The techniques and methods implemented to characterize and diagnosis the bearing faults are numerous and very diverse, these techniques can be grouped into three families, frequency domain methods as Fast Fourier Transform (FFT), temporal statistical methods as Kurtosis and filtering method as high pass (G.Y. Massala Mboui,2018). In the present thesis, Fast Fourier Transform (FFT) is used to detect and diagnose the ball bearing faults.

Motor Current Signature Analysis (MCSA) are used in this work for detecting the bearing faults in IM, this technique can be used to examine the supply currents for detecting a particular motor failure while running, it consists of using the spectrum of the stator current of the machine to locate and characterize the fault frequencies, when fault occurs, the spectrum of the line current becomes behaves different from healthy motor case (N. Mehala, 2010)

I.2 Aim and objective of the study

The main aim of this study is to diagnose and detect ball bearing faults in induction motor. For this purpose, several steps have been achieved as follows:

- Modeling the squirrel cage induction motor and the ball bearing on MATLAB software.
- Applying different faults to the bearing model (outer race and inner race),
- Relating faulted ball bearing model to the IM model,
- Applying signal processing method (FFT) on different signals (current, torque, speed, acceleration).

I.3 Format of the dissertation

The dissertation is divided into six chapters: Chapter two introduces the induction motor machine, its different failure modes and condition monitoring techniques to detect these failures. Chapter three presents the modeling methods of the machine, in which the coupled circuit method is used in this study followed by the model of ball bearing as well as the effect of bearing defects on the operation of the machine and its influence on the mechanical and electrical quantities. Chapter four is dedicated to present time-domain simulation results of the induction motor model. Chapter 5 discusses the frequency domain simulation results obtained from spectral analysis based on Fast Fourier transform. Chapter 6 presents the conclusion and recommendations for further investigation.

CHAPTER II

NOTIONS AND RELATED STUDIES

II.1 INTRODUCTION

The induction machine (IM) both stator and rotor carry alternating currents. Alternating current is supplied to the stator winding directly while the currents to the rotor are induced by electromagnetic induction phenomenon, hence the name induction machine.

Squirrel-cage induction motor is economical and robust as compared to the wound-rotor induction motor type, at constant supply voltages and frequency, it run at a constant speed. For this type of motor, if there is an increase in the load torque, the speed will decrease slightly (N. Saad, et al, 2019). The particular reasons for this acquired confidence in the IM are based on its intrinsic qualities such as its simplicity of construction, its mechanical robustness and its low cost of purchase and manufacture. However, IM are often operating in harsh environment such as in insufficient cooling areas, inadequate lubrication, structure vibration, overload, frequent motor starts and stops, magnetic fatigue caused by electromagnetic forces and excessive heating. This environment frequently causes defects in different parts of the machine, such as breaks in rotor bars, stator short circuits, eccentricity caused by the bearing faults … etc.

In this chapter, the structure of IM along with the bearing types in rotating machinery is briefly described. In addition, electrical (stator and rotor) and mechanical (bearing, eccentricity, flange) faults are presented in this chapter.

II.2 Induction Machine Structure

The IMs are physical devices composed mainly of stator, rotor and mechanical parts such the bearings that support smooth rotating machine (A. Bouzida, 2015)

- The stator (fixed part) made up of magnetic sheet discs carrying the windings responsible for magnetizing the air gap.
- The rotor (rotating part) carries bars permanently short-circuited by the end rings.

- The mechanical parts allowing the rotation of the rotor and the maintenance of the different sub-assemblies.

II.2.1 Stator

The stator of the asynchronous machine is made of steel sheets in which are placed the stator windings. These sheets are, for small machines, cut into one single part whereas, for larger power machines, they are cut by sections. They are usually covered with varnish to limit the effect of Eddy's currents. Ultimately, they are assembled to each other using bolts or welds to form the stator magnetic circuit. Once this assembly step is completed, the stator windings are placed in the notches provided for this. These windings can be inserted in a nested, wavy or even concentric way.

The concentric winding is very often used when the windings of the asynchronous machine is carried out mechanically. For large machines, the windings are made of copper flats of different sections inserted directly into the notches. Insulation between the electrical windings and the steel sheets is carried out using insulating materials which can be of different types depending on the use of the asynchronous machine. The stator of an asynchronous machine is also provided with a terminal box in which the power supply is connected. The different constructive parts of the stator of an asynchronous machine are represented in the figure II-1 (A. Bouzida, 2015).

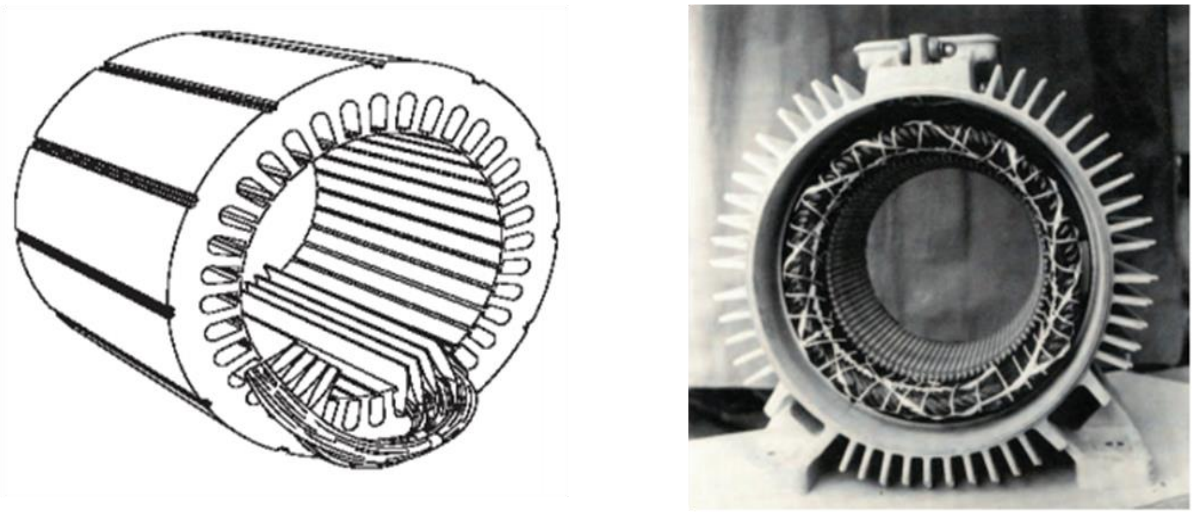

Figure II.1: (a) Stator being wound and (b) stator (overview)

II.2.2 Rotor

Similar to the stator, the rotor magnetic circuit is made of steel sheets which are in general, of the same origin as those used for the construction of the stator. The IM rotors are found into two types: wound or squirrel cage.

The wound rotors are constructed in the same way as the stator winding (insertion windings in the rotor slots). The supply to rotor phases is then available with the help of the brush rings positioned on the machine shaft (A. Bouzida, 2015). In the other hand, squirrel cage winding is depending on the power of the machine, notches in the rotor cage for low power machines are generally in the form of oval which are filled with cast aluminum forming the bars of the cage. The short circuit rings are also obtained by casting aluminum on both side of the rotor. For high power machines, the rotor has deep notches, bars are made of copper and have a rectangular section, and the short-circuit rings are most often made of copper also, they are welded to form the rotor cage (S. Hamdani, 2012).

Various cage rotor structures exist which mainly depend on the size of the machine and its application. As presented in figure II.2, the sheets are stacked; the two short-circuit rings as well as the aluminum bars forming the squirrel cage. Very often these bars are evenly angled to limit harmonics and thus greatly reduce noise when accelerating the machine.

Insulation of the bars with the magnetic sheets is generally not necessary because of the low voltage induced at the terminals for each of them. In addition, the resistivity of the alloy used for the construction of this cage is weak enough so that the currents do not flow through the magnetic sheets, except when the rotor cage presents a bar break. The rotor of the IM also contains fins of ventilation to allow good cooling of the cage as shown in figure (A. Bouzida, 2015)

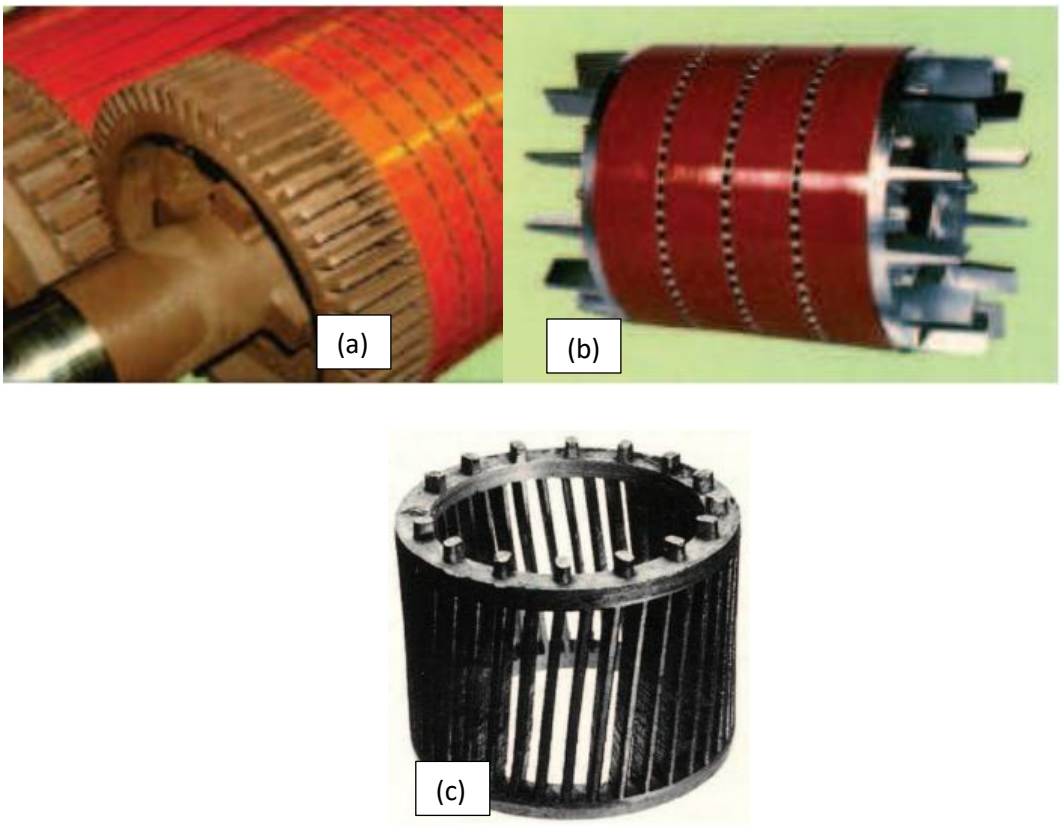

Figure 0.1: (a) Copper bar rotor, (b) aluminum bar rotor Squirrel-cage rotor (M.E.K. Oumaamar, 2012)

II.2.3 Bearings

The bearing is a basic member which provides a movable connection between two elements of a rotating mechanism relative to each other. Its function is to allow the relative rotation of these elements under load with precision and with minimum friction. Ball bearing is the most used type in the industrial world due to its good-performance (A. Ibrahim, 2009)

Bearing is made up mainly of three elements listed as follows

- Two concentric steel rings, called the inner ring and the outer ring, comprising raceways (surfaces on which the bodies "roll" rolling);
- Rolling bodies, balls or rollers generally made of steel, allowing the movement of the two rings with minimal friction, placed in raceways rotates inside the rings
- A cage separating and guiding the rolling bodies (in polyamide, sheet steel, brass or resin).

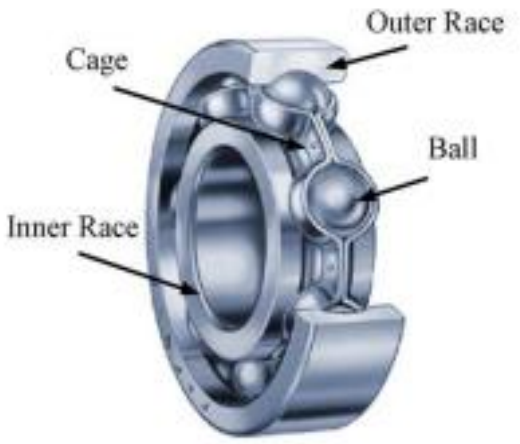

Figure 0.2 : Ball bearing (Izzet, et al, 2008)

II.2.3.1 Types of bearings

There are several types of bearings, including ball bearing, roller bearing, linear bearing, fluid bearings, magnetic bearing and plain bearings. In this sub-section, a brief description of the two most common types is addressed.

II.2.3.1.1 Ball Bearing

The ball bearing (Figure II-4) is the most common type of bearings. It consists of small metal balls that are located between two metal rings which are known as Races. Balls are kept in uniform space position using an assembly called Cage. Since sliding friction is high compared to rolling friction, ball bearing provides less energy loss. The inner races and balls are free to rotate while the outer race is stationary. The shaft is fitted inside the inner race and the outer race is fixed to a motor or the housing of the mechanism.

Figure 0.3: Ball bearing

Ball bearings are superior in use due to their advantages as they are less resistive, easy to replace, less cost, handle high loads and live longer. On the other hand, this type of bearing is quite noisy and can get defected with excessive shocks and loads.

II.2.3.1.2 Roller Bearings

Roller bearings (Figure II-5) are usually used for applications requiring exceptionally large load-supporting capabilities, which cannot be feasibly, obtained using ball bearing assemblies. Roller bearings are usually much stiffer structures (less deflection par unit loading) and provide greater endurance than ball bearings do. They usually require great care in mounting. Accuracy of alignment shafts and housings can be a problem in all but self-aligning roller bearings (T. Harris, et al, 2007)

Figure II.5: Roller bearing

The advantages of this type of bearing can represent in their low friction, high load capacity and easy maintenance. As disadvantages, this type of bearing is very noisy and costly as well.

II.3 Different faults in the induction machine

Due to the simplicity in construction with fewer parts which reduce the maintenance cost, the IMs are the major drives used in industry, although they are robust the induction machines are exposed to different environmental factors which are not always ideal and sometimes even harsh, such as in insufficient cooling areas, humidity, inadequate lubrication, structure vibration, overload, frequent motor starts and stops. Faults generally disturb the symmetry of the motor between the stator and the rotor, the usual symptoms related to disturbed symmetry are: reduction in efficiency, unbalanced air-gap, voltages and line currents, increased space harmonics, a decreased shaft torque, an increased torque pulsation, and increased losses (A. Bouzida, 2015), (N. MEHALA, 2010). Statistics shows that faults with mechanical origin represent 70% while faults from electrical origin represent about 30% from the total faults in IMs (see Figure II-6).

The use of induction motor under faults certainly disturbs their performances and reduces their remaining useful life (P.S. Bhowmik, et al, 2013).

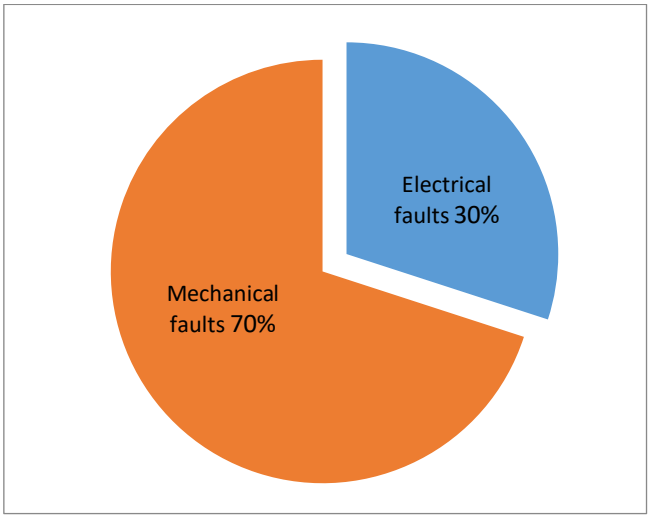

Figure II.6: Results failures distribution

II.3.1 Electrical failures

Failures of electrical origin can in certain cases be the cause of shutdown of the machine (in the same way as mechanical failures). These failures can be separated into two distinct categories: failures which appear at the level of the stator electrical circuits and those which appear at the level of the rotor electrical circuits (G. Didier, 2004).

II.3.1.1 Stator Faults

Stator faults can be classified as (i) faults in laminations and frame of stator and (ii) faults in stator winding. Under an EPRI project, a survey of large electric motors Utility, the study found that stator winding failure is one of the main causes of motor failure. As per the study of IEEE and EPRI, 28–36 % of induction motor faults are stator winding fault. Majority of these faults are due to a combination of the various stresses such as mechanical, electrical, thermal, and environmental. Other Work shows that most motor stator winding failures are caused by the destruction of the turn insulation (S. Karmakar, et al, 2016). Different types of stator winding faults are (i) short circuit between two turns of the same phase called turn-to-turn fault, (ii) short circuit between two coils of same phase called coil to coil fault, (iii) short circuit between turns of two phases called phase to phase fault, (iv) short circuit between turns of all three phases, (v) short circuit between winding conductors and the stator core called coil to ground fault, and (vi) open-circuit fault when winding gets break. Different types of stator winding faults are shown in Figure II-6. Among the five failure modes, steering failure (stator rotation failure) is considered the most difficult, because other types of failures are usually the result of rotation failures. In addition, it is difficult to detect steering failures at its initial stage. *(*J. Penman, et al, 1994)(S. Karmakar, et al, 2016).

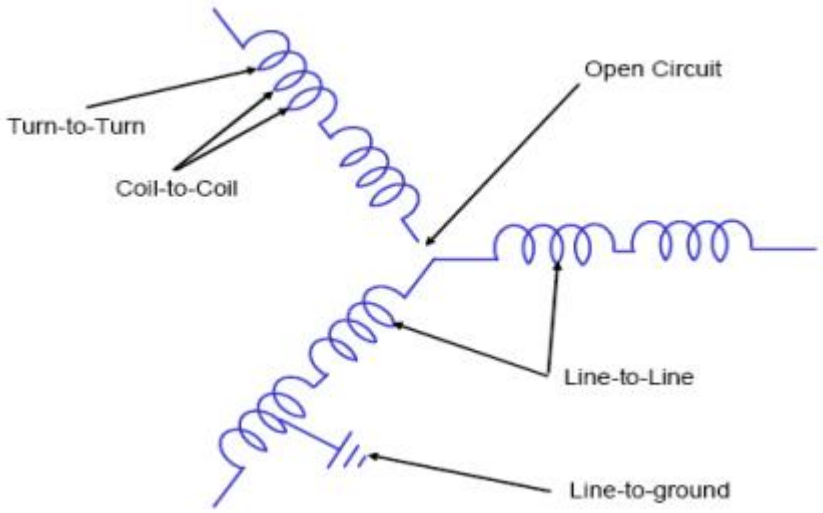

Figure II.6: various types of short winding faults (N. Mehala, 2010)

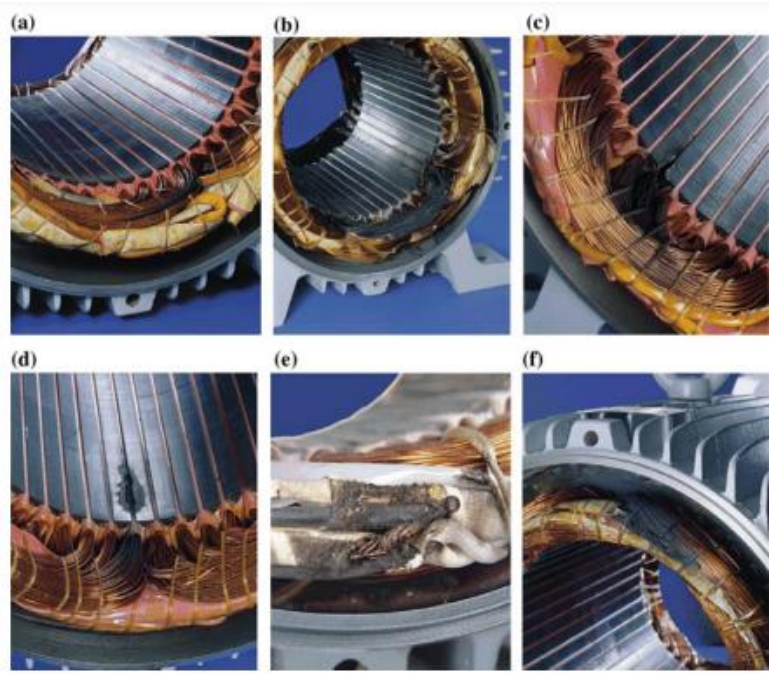

Figure II.7: Typical insulation damage leading to inter-turn short circuit of the stator windings in three-phase induction motors. (a) Inter-turn short circuits between turns of the same phase. (b) Winding short circuited. (c) Short circuits between winding and stator core at the end of the stator slot. (d) Short circuits between winding and stator core in the middle of the stator slot. (e) Short circuit at the leads. (f) Short circuit between phases

II.3.2 Causes and Effects of Stator Winding Faults

As mentioned earlier, IMs are subjected to various stresses such as mechanical, electrical, thermal, and environmental. Mechanical stress as high vibration can disconnect the stator winding that produces open circuit failure, the top sticks may get loose and the copper conductor and its insulation may get damaged due to coil movement. The rotor also may strike the stator due to rotor-to-stator misalignment, shaft deflection, bearing failure. Electrical stresses are mostly due to the supply voltage transient which in turn reduces the endurance of the stator windings and in severe case may cause turn-to-turn or turn-to-ground fault. Lightning, opening or closing of circuit breakers, variable frequency drives may also cause electrical stress (A. Siddique, 2005).

In addition, thermal stresses are the principal reason for insulation of the stator winding, thermal overloading is the mainly reasons of thermal stresses, moreover, over current flowing due to sustained overload or fault, higher ambient temperature, obstructed ventilation, unbalanced supply voltage cause thermal stress, the number of starts and stops within a short time are made in the motor increase the temperature of windings. If the motor is operated over its temperature limit the best insulation may also fail quickly. As a rule of thumb, for every 10 °C increase in temperature above the stator windings temperature limit, the insulation life is reduced by 50 % (A.H. Bonett, 1992). Finally, motor operation in a hostile environment with too hot or too cold or too humid irises environment stresses. Furthermore, the presence of foreign material can contaminate insulation of stator windings and also may reduce the rate of heat dissipation from the motor (S. Karmakar, et al, 2016).

II.3.3 Rotor Faults

The squirrel cage rotor of the induction machine compound of bars and short-circuit rings being made of aluminum or copper. Therefore, the faults which are more recurring, localized at the level of the rotor of the IMs can be either broken bars or broken end-rings (A. Bouzida, 2015).

A partial or total rupture of one of these components can be considered as a rotor electrical fault. Rotor failures now account for a large percentage of all induction motor failures, the main reasons for the rotor bar and end ring, breakage are thermal stress due to thermal overload and unbalance, sparking or excessive losses. Magnetic stresses caused by

electromagnetic forces, unbalanced magnetic pull (UMP), electromagnetic noise and vibration. Residual stresses due to manufacturing problems. Dynamic stresses arising from shaft torque, centrifugal forces and cyclic stresses. Environmental stresses caused by contamination or abrasion of the rotor materials due to chemicals or moisture. And mechanical stresses due to loose laminations, fatigued parts or bearing failure.

The reasons mentioned above could cause damage to the bars of the rotor and at the same time cause the rotor to become unbalanced (N. Saad, 2019).

II.3.3.1 Broken bar fault

Rotor bar breakage is one of the most common rotor faults. It can be located either at its notch or at the end which connects it to the short-circuit ring. Damage to just one rotor bar could result in damage to the surrounding bars because of asymmetrical rotor currents witch are produced due to asymmetry of the cage of the rotor (N. Saad, 2019). The deterioration of the bars reduces the average value of the electromagnetic torque and increases the amplitude of the oscillations or ripples, which themselves cause oscillations in the rotational speed, that leads to mechanical vibrations and therefore abnormal operation of the machine. The large amplitude of these oscillations accelerates the deterioration of the machine (B. Vaseghi, 2009). Thus, the torque decreases appreciably with the number of broken bars inducing a cumulative effect of the failure. One or more broken bars cause an imbalance of the rotor current, which is composed of two direct and inverse systems (S. BELHAMDI, 2014).

The inverse system creates a rotating field at the frequency $(-fg)$ with respect to the rotor and ($f - 2fg$) with respect to the stator. It will induce a stator current of frequency (f-2fg) different from that of the network. For the same reason, we will have a stator current which comprises components frequency presented as side bands (S. BELHAMDI, 2014).

$$f_{bc} = (1 \pm 2kg)\, f \qquad \text{(II-1)}$$

On the other hand, the space harmonics also generate frequencies given by

$$f_b = f\left\{1 \pm k\frac{(1-g)}{P}\right\} \quad \text{(II-2)}$$

k: Odd integer.

f: Supply frequency.

g: Slipping.

f_{bc}: frequency generated by the fault.

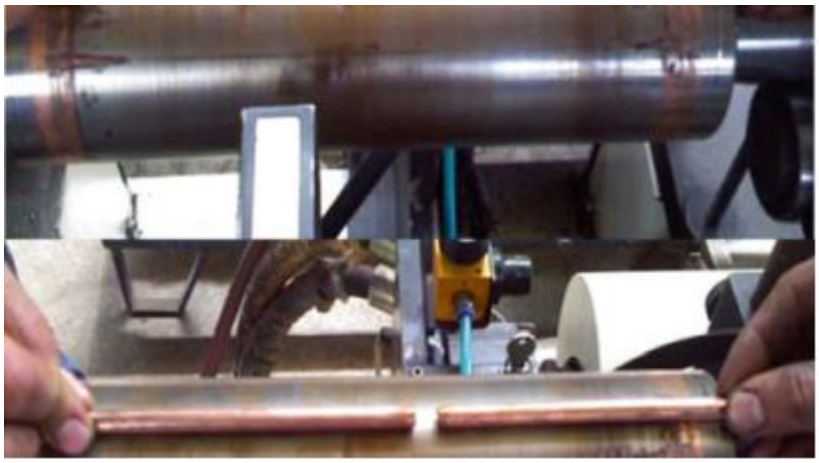

Figure II.8: Photograph of rotor and parts of broken rotor bar (S.Karkmar, et al, 2016)

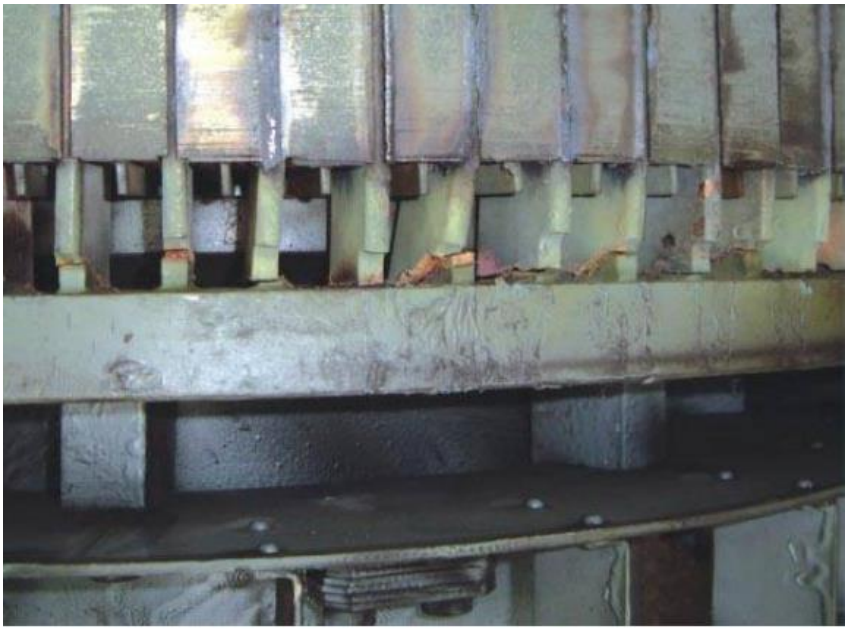

Figure II.9:(A.Bouzida,2015)

II.3.3.2 Breaking of short-circuits rings

The rupture of a portion of the short-circuit ring in IMs is a fault which appears as frequently as the breaking of bars. These ruptures may be due to flow bubbles or to differential expansions between the bars and the rings. As it is difficult to detect, this defect is generally grouped, even confused with the breakage of bars in statistical studies. These portions of short-circuit rings convey currents greater than those of the rotor bars. As a result, poor sizing of the rings, deterioration of operating conditions (temperature, humidity, ...) or an overload of torque and therefore of currents, can cause them to break. The rupture of a ring portion unbalances the distribution of the currents in the rotor bars and therefore generates an amplitude modulation that effect on the stator currents similar to that caused by the breakage of the bars (B. Vaseghi, 2009).

II.3.4 Mechanical defect

Mechanical components are the most significant part of the electrical motor that are continuously exposed to an increased wear. This is confirmed by different researcher in surveys where approximately 70% of failures are of mechanical origin. These faults can appear at the level of the ball bearings, the flanges or even the rotor shaft.

II.3.4.1 Flange failures

The faults created by the flanges of the IMs are generally caused during the manufacturing stage. Indeed, a bad positioning of the flanges causes misalignment of the ball bearings, which induces an eccentricity at the level of the shaft of the machine. It is possible to detect this type of failure by vibration analysis or a harmonic analysis of the currents absorbed by the machine (G. Didier, 2004)

II.3.4.2 Shaft failures

The machine shaft may show a crack due to the use of wrong material in its construction. In short or long term, this crack can lead to an irreparable stop of the machine. There are informal studies suggest that fatigue-caused failures are much higher; it climbs into the 90% range when the effects of corrosion and new stress raisers are considered. The shaft fatigue failures can be classified as bending fatigue, torsional fatigue, and axial fatigue. In the case of axial fatigue, the bearing carrying the load will get fatigue (contact fatigue) before the shaft does. This is usually evidenced by spelling of the bearing raceways. In the bending mode, almost all failures are considered “rotational” with the stress fluctuating or alternating between tension and compression. This is a cycling condition that is a function of the shaft speed. Torsional fatigue is associated with the amount of shaft torque present and transmitted load. In addition, corrosion weakens the strength of the shaft; at the core of this problem is an electrochemical reaction that weakens the shaft. Pitting is one of the most common types of corrosion, which is usually confined to a number of small cavities on the shaft surface this pitting caused a crack (A. H. Bonnett, 2000). Humidity also can cause micro-cracks and lead to complete destruction of the machine. A static, dynamic or mixed eccentricity can induce considerable forces on the motor shaft, thus causing additional fatigue. Vibration analysis, ultrasound analysis, frequency analysis of the absorbed currents or simply a visual analysis of the machine shaft can detect this type of failure (G. Didier, 2004).

II.3.4.3 Air-Gap Eccentricity defects

In this kind of faults, the symmetrical axes of rotor and stator lose their conformity and the air gap becomes non-uniform. Almost 80% of the mechanical faults are due to the rotor and stator eccentricity (H.A. Toliyat et al, 1999). Eccentricity faults cause not only variation in the

air gap but also the non-homogeneous distribution of the currents in the rotor as well as the imbalance of the stator currents.

Eccentricity faults usually produce noise and vibration in the motor. where the center of the rotor and stator bore should perfectly aligned in healthy motors. Moreover, the center of rotation for the rotor is the same as the stator bore center. If the rotor is not aligned centrally, radial forces or magnetic pull will be developed. The imbalance of the forces on the bars generates an overall non-constant torque. When the eccentricity becomes large, the resulting radial forces created by the stator with the friction strip of the rotor cause damage to the stator and the rotor (A. Bouzida, 2015) (N. Saad, 2019). The sideband frequencies associated with an eccentricity using Motor Current Signature Analysis are (M. Sahraoui et al, 2008):

$$f_1 = \left[\left(kN_r \pm n_d \right) \frac{(1-s)}{p} \pm v \right] f_s \qquad \text{(II-3)}$$

where k is any positive integer, N_r is the number of rotor slots, n_d = 0 in case of static eccentricity and n_d = 1, 2...

Some causes of this phenomenon can be: bent shafts, wear on the bearings, mechanical vibrations or resonances (A. J. Bazurto, et al, 2016).

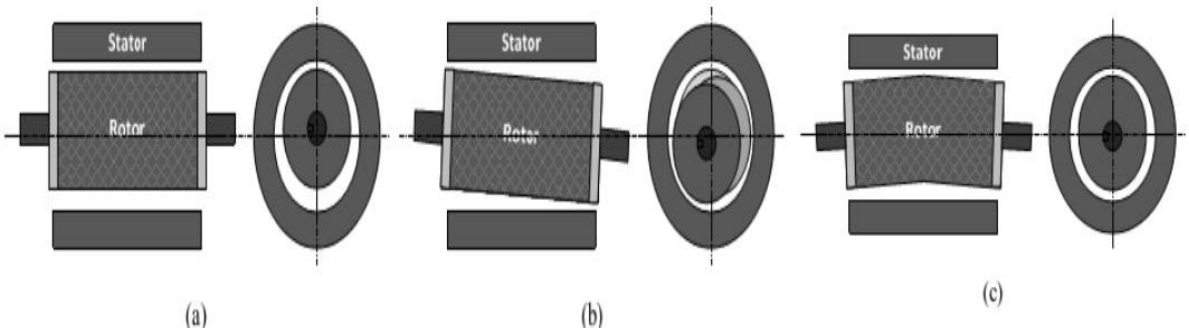

Figure II.10: (a) static eccentricity and (b) dynamic eccentricity faults (c).

II.3.5 Types of Eccentricities

There are three kinds of air-gap eccentricities: the static air-gap eccentricity, the dynamic air gap eccentricity and mixed air gap eccentricity (S. Nandi et al, 2005).

II.3.5.1 Static air-gap eccentricity

In this case of air-gap eccentricity, the rotational axis of the rotor is identical to its symmetrical axis but has been displayed with respect to the stator symmetrical axis. Moreover, the air gap distribution around the rotor is not uniform, it is time-independent. If the rotor-shaft assembly is sufficiently stiff, the level of static eccentricity does not change

The reasons for increasing the eccentricity are as follows:

- Bad position of the stator core when mounting the motor, or
- Non-orientation of the stator and rotor centers during basic maintenance.

II.3.5.2 Dynamic air-gap eccentricity

In case of dynamic eccentricity, the minimum air gap length depends on the rotor angular position, and it rotates around the rotor. The center of the rotor is not at the center of the rotation and the position of minimum air-gap rotates with the rotor and time varying. Several factors such as a bent rotor shaft, bearing wear or misalignment, mechanical resonance at critical speed, may cause the misalignment.

II.3.5.3 Mixed air-gap eccentricity

The mixed eccentricity is the existence of both static and dynamic eccentricity. In this case, the symmetry axis of the rotor and stator and the rotation axis of the rotor are displaced.

II.3.6 Bearing failures

All the forces of a shaft line are supported and received by the bearings, thus they are the most critical elements of a machine. Bearings are undoubtedly the most sensitive parts of a machine. Ball bearings are the most used in industry they act as an electromechanical interface between the stator and rotor. In addition, they represent the element of maintenance of the axis of the machine to ensure good rotation of the rotor.

Almost 40%–50% of all motor failures are bearing related (S. Nandi, et al, 2005). Bearing defects can occur during material fatigue under normal operating conditions. At first, cracks will appear on the tracks and on logs. Second, chipping and pulling of material can quickly accelerate bearing wear (A. Ibrahim, 2009).

Flaking or spelling of bearings might occur when fatigue causes small pieces to break loose from the bearing. Beside the normal internal operating stresses caused by vibration, inherent eccentricity, and bearing currents due to solid state drives, bearings can be spoiled by many other external causes such as 1) Contamination of the bearing by external particles: dust, grains of sand, 2) Corrosion caused by the penetration of water, acid, 3) Inadequate lubrication which can cause overheating and wear of the bearing, 4) Misalignment of the rotor, 5) Current flowing through the bearing and causing electric arcs, and 5) Incorrect installation of the bearing; by incorrectly forcing the bearing onto the shaft of the rotor or in the flanges (due to misalignment), notches will be formed on the raceways.

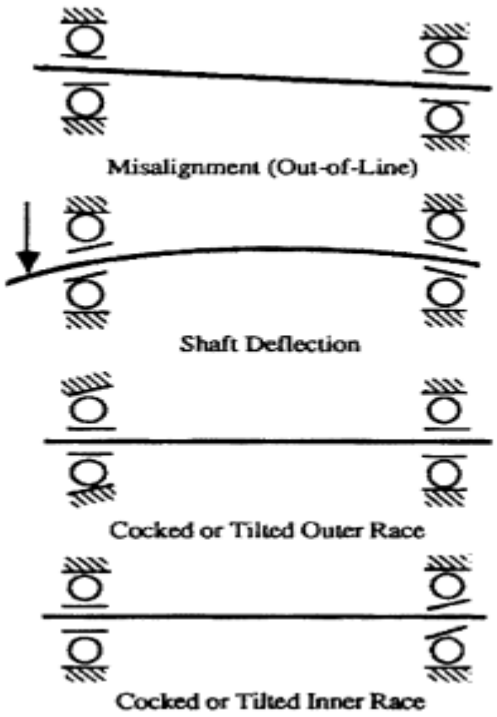

Figure II.11: Four types of rolling-element bearing misalignment (M.E.H. Benbouzid, et al, 1999)

The relationship of bearing vibration to stator current spectrum results from the fact that any air gap eccentricity produces anomalies in the air gap flux density. The characteristic vibration frequencies due to bearing defects can be calculated from the rotor speed and the bearing geometry. The typical rolling element bearing geometry is displayed in the figure bellow (Figure II-12).

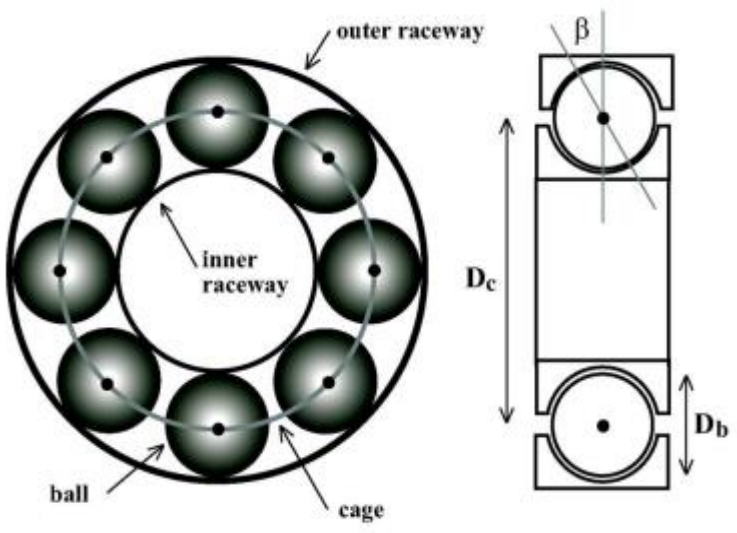

Figure II.12: Geometry of rolling element bearing (M. Blödt, et al, 2008)

A single-point defect could be imagined as a small hole, a pit, or a missing piece of material on the corresponding element. With each type of bearing fault, a characteristic frequency f_c can be associated. This frequency is equivalent to the periodicity by which an anomaly appears due to the existence of the fault. For instance, a hole on the outer raceway, when the rolling elements move over the defect, they are regularly in contact with the hole, which produces an effect on the machine at a given frequency. The characteristic frequencies are functions of the bearing geometry and the mechanical rotor frequency (M. Blödt, et al, 2008)

The outer race defect frequency, f_O, the ball passing frequency on the outer race, is given by:

$$f_o = \frac{N_b}{2} f_r \left(1 - \frac{D_b}{D_c} \cos\beta\right) \quad \text{(II-4)}$$

Where β is the contact angle, D_c is the pitch diameter, D_b is the ball diameter, N_b is the number of balls, and f_r is the rotational frequency.

The inner race defect frequency, f_i the ball passing frequency on the inner race, is given by

$$f_i = \frac{N_b}{2} f_r \left(1 + \frac{D_b}{D_c} \cos\beta\right) \quad \text{(II-5)}$$

The ball defect frequency, f_b the ball spin frequency, is given by

$$f_b = \frac{D_c}{D_b} f_r \left(1 - \frac{D_b^2}{D_c^2} \cos^2\beta\right) \quad \text{(II-6)}$$

The train defect frequency, f_T caused by an irregularity in the train, is given by

$$f_T = \frac{1}{2} f_r \left(1 - \frac{D_b}{D_c} \cos\beta\right) \quad \text{(II-7)}$$

The vibration frequencies can be approximated for most bearings with number of balls between 6 and 12 balls by:

$$f_o = 0.4 N_b f_r \quad \text{(II-8)}$$

$$f_i = 0.6 N_b f_r \quad \text{(II-9)}$$

The most often cited model studying the influence of bearing damage on the stator current of induction machine was proposed by Schoen et al (R. Schoen, et al,1995). The authors consider the generation of rotating eccentricities at bearing fault characteristic frequencies f_c, which leads to periodical changes in the machine inductances. This should produce additional frequencies f_{bf} in the stator current, which is given by

$$f_{bf} = |f_s \pm k f_c| \quad \text{(II-10)}$$

Where, f_s is the electrical stator supply frequency, and $k = 1, 2, 3...$

II.4 Condition Monitoring

Condition monitoring is characterized as the persistent assessment of the wellbeing of the manufacturing process or particularly a rotating machine as it is critical to distinguish deficiencies while operating. This may result in decreasing down time and ideal maintenance plans. Condition monitoring and fault diagnosis permits the machine's operator to have the fundamental parts being saved some time recently the machine is stripped down, therefore lessening blackout time. Subsequently, successful condition monitoring of induction machines is basic in moving forward the reliability, safety, and productivity (N. Mehala, 2010). Advantages of using condition monitoring can be mentioned point wise as below (S. Karmakar, et al, 2016):

- Can predict the motor failure.
- Can optimize the maintenance of the motor.
- Can reduce the maintenance cost.

- Can reduce downtime of the machine.
- Can improve the reliability of the motor.

II.4.1 Existing Techniques for Fault Analysis of Induction Machine

There are a number of techniques that have been applied in detecting mechanical failures in rotating machinery. In this subsection, we briefly describe the most common techniques.

II.4.1.1 Thermal Analysis

Fault detection of an induction motor by thermal analysis is practiced by measuring the change its temperature. The thermal monitoring of induction motors is accomplished firstly by taking measurement of the bulk temperature, or the local temperature of the motor; and secondly, by performing an estimation of the parameter. Thermal analysis can be used to detect bearing fault and turn-to-turn stator winding fault of an induction motor. In case bearing fault, friction increases which in turn increases the temperature of the motor. In case of turn-to-turn fault temperature increases in the fault region, as a result detection of the fault would take time. Thermal analyzing this change in temperature motor fault can be predicted (S. Karmakar, et al, 2016)(N. Saad, et al,2019).

II.4.1.2 Chemical Analysis

The heat causes the degradation of lubricants which produces a large number of chemicals in solid, liquid and gas form. Bearings also produce debris; therefore, oil and greases lubricants not have only their own degradation materials but also transport the debris of the bearings. Chemical analysis can only be performed if the oil lubricants and greases are available, though the analysis of these greases can be used as a diagnostic and fault condition monitoring for bearings (N. Saad, et al,2019), it's only used with big motors and not with the typical small ones (J. Cusido,et al,2011).

II.4.1.3 Acoustic Analysis

Acoustic analysis is performed by measuring and analyzing the acoustic noise spectrum (N. MEHALA, 2010), this analyze can be used for fault detection in induction motor because this spectrum may change when faults like bearing fault, air gap eccentricity fault occur (S. Karmakar, et al, 2016).Acoustic analysis consist in recording acoustic signals using a digital voice recorder or online by using microphone with a computer. However, there is no

practicality in applying noise measurements in an industrial plant as the other machinery running in the vicinity will make the background too noisy, so the accuracy of the fault detection would be reduced due to the background noise (N. Saad, et al, 2019). Moreover, there are some advantages such as: easy access to acoustic signal, inexpensive microphone, it is possible to analyze electrical and mechanical faults like shorted windings, broken bars, bearings, rotor shaft, etc. (A. Glowacz, 2019)

II.4.1.4 Torque analysis

Most of the faults in an induction motor produce harmonics of specific frequencies in the air gap. But this air gap torque cannot be measured directly. Also the air gap torque is different from the torque measured at the shaft of the motor. Air-gap torque represents the combined effects of all the flux linkages and currents in both the stator and the rotor of the entire motor. It is sensitive to any unbalance created by defects as well as by unbalanced voltages, it tells distinctively whether the unbalance is caused by cracked rotor bars or by stator unbalance associated with winding defects and unbalanced voltages. It is important to use previous measurements under the same unbalanced voltages as references to indicate defects developed in the induction motor (J. S. Hsu,1995). In terms of motor terminal parameters which are measurable, air gap torque in Newton-meter could be expressed as (S. Karmakar, et al, 2016)

$$\Gamma = \frac{p}{\sqrt{2}}\left[\left(i_a - i_b\right)\int\left[V_{ca} - R\left(i_a - i_b\right)dt\right] - \left(i_c - i_a\right)\int\left[V_{ab} - R\left(i_a - i_b\right)dt\right]\right] \quad \text{(II-11)}$$

Where, i_a, i_b and i_c are line currents of the induction motor, V_{ab} and V_{ca} are line-to-line voltages, p is number of pole pairs, and R is half of the line-to-line resistance.

II.4.1.5 Induced Voltage Analysis

In S. Karmakar, et al (2016), fault can be identified by analyzing the induced voltage along the shaft of a machine, this voltage is induced due to degradation of insulation of stator winding. Generally, this induced voltage is very small and is measurable when a large degree

of damage in the stator winding occurs. Due to this reason, induced voltage method is not widely used.

II.4.1.6 Partial Discharges Analysis

Partial discharges (PD) are small sparks that occur in high voltage insulation wherever small air pockets exist, thus since overloading, coil vibration and pollution create pockets, PD is a symptom of most high voltage stator winding failure processes. So partial discharges are used for detecting stator insulation faults in higher voltage motors where the testes can be performed off-line when the machine is not operating or on-line during normal operating of the motor or generator (G. Stone, et al, 1998).Gradual degradation of stator insulation will lead to increased partial discharge activity, but a quantitative relationship between that activity and the remaining life of the insulation, which is needed for condition monitoring, has not yet been established and may prove difficult to demonstrate. Even under laboratory conditions, the prediction of remanent life for electrically stressed specimens does not have the accuracy needed. Discharge monitoring techniques, however, have been much more widely applied to generators where damaging discharge activity is a more common precursor of major faults and the financial benefits of obtaining this warning are greater (P.J. Tavner, et al, 1986).

II.4.1.7 Vibration analysis

The vibration analysis is very old method and one of the most important methods used for fault diagnosis in electrical machine. All electrical machines produce noise and vibrations. Analyses of the vibration signal of the motors are used to detecting the different kinds of defects and asymmetries. More often, measurements are made as an infrequent procedure or when a problem is suspected, they are made using accelerometers or speed at bolts (A. Chaouch, 2013). Magneto-motive and mechanical forces are the cause of noise and vibrations in motors where the radial forces resulting from the air-gap field are the greatest sources of vibrations in the motors. The resultant magneto-motive force waves and total permeance wave generate the air-gap flux density distribution. The resultant magneto-motive force possesses the effect of potential stator or rotor asymmetries and permeance wave is dependent upon the differences of the air gap. The most suitable situations for performing diagnostics based on vibration analysis are in situations of analysis of bearings and gear faults (N. Saad, et al, 2019). Vibration fault diagnostic techniques have many advantages which are: inexpensive

accelerometer, immediate measurement of the vibration signal, it is possible to analyze electrical faults shorted windings, broken bars, faulty ring of squirrel-cage and mechanical faults like bearings, rotor shaft, easy access to vibration signal. Furthermore, disadvantages of this technique are: set of accelerometer should be very close to the motor and set of accelerometer/data logger should be the same (measurement in the axes X, Y, Z), (A .Glowacz, 2019).

II.4.1.8 Analysis of Stator Currents

Among all the usable signals, the stator current proved to be one of the most interesting, because it is very easy to access and makes it possible to detect both electrical and purely mechanical faults. This technique is referred to in the literature as "Motor Current Signature Analysis" (MCSA). The faults of the asynchronous machine are reflected in the stator current spectrum either by (A.Bouzida,2015):

- The appearance of spectral lines whose frequencies are directly linked to the machine's rotation frequency, the frequencies of the rotating field, the physical parameters of the machine (number of rotor notches and number of pole pairs).
- Modifying the amplitude of spectral lines already present in the current.

It has several advantages over other methods, because it requires neither the introduction of a sensor at the machine nor the use of expensive and bulky equipment but only a current sensor (Hall Effect probe or current transformer) which gives an image on the stator phase current. It is a method of monitoring, which consists of using the spectrum of the stator current. Knowing that in a current spectrum of a faultless motor appears only the component of the fundamental, for a sinusoidal distribution of the magneto-motive force, in the case of a non-sinusoidal distribution of the magneto-motive force in addition to the fundamental appears harmonics of the rotor notch, case of a cage motor (A. Chaouch, 2013).

II.5 Summary

In this chapter, we have recalled the constructive elements of the asynchronous squirrel cage machine and we have also described the majority of the faults that can occur as well as their influences on the machine, finally mentioning some types of the diagnostic techniques for these faults.

CHAPTER III

INDUCTION MACHINE/BALL BEARING MODELLING

III.1 Introduction

This chapter presents the modeling of the IM as well as the model of the ball bearing. First, we discuss the common methods used to model the induction machine. Then we introduce the essential tools for the resolution of the chosen model. Then the development of the mathematical model of ball bearing and defect generation is presented subsequently. Finally, we will see the effects of the bearing faults on the machine and how mechanical information transfer to the electrical quantities.

III.2 Modeling methods of Induction Machine

The models that describe the operation of the IM can be decomposed into two distinct parts: Physicals models and behavioral models. (G. Didier, 2004). Regarding to physical models, the laws governing electromagnetism are used to describe the functioning of the asynchronous machine. These models are diverse and may vary in complexity and/or accuracy depending on the modeling method used. We will mention the most popular methods including those based on: 1) Finite element method, 2) Permeance network method, and 3) Magnetically coupled electric circuit method

Behavioral models, on the other hand, replicate physical models with additional parameters. These parameters allow the detection, and the localization of the observed defect.

III.2.1 Finite Element Method

Finite element analysis is a numerical technique for calculating the parameters of electromagnetic devices; it can be used to calculate the flux density, flux linkages, inductance, torque, induced EMF (Electromagnetic induction) etc. It is the most suitable and widespread method for the calculation of static or quasi-static magnetic fields, it allows to accurately describe complex geometries. This method is able to examine the saturation effect and the harmonic effects of space. Moreover, the magnetic circuit of the machine is decomposed into

many small elements to allow the linear magnetic material to be considered on the corresponding surfaces, and gives a lot of precise information on the behavior of electrical machines, but it requires a significant computing time. The computer can solve this large set of simultaneous equations, the problem solved using Maxwell's equations local forms, from the solution, the computer extracts the behavior of the individual elements (B.Vaseghi. 2009)(G. Didier.2004) (W. Zaabi, et al, 2014).

III.2.2 Permeance Network Method

The permeance network method is based on the decomposition of the magnetic circuit of the electric machine in elemental flux tubes characterized by their magnetic permeances (A. Mahyob, et al, 2009). From this decomposition, we build a network called permeance. These networks can be likened to a usual electrical circuit to the difference except that the flows and differences of magnetic potentials replace currents and differences of electrical potentials. This approach allows taking into account the characteristics of the iron used for the construction of the asynchronous machine. The calculation of the different permeances can only be done by fixing a precise value for the relative permeability of the iron μ_r. The rotation movement of the machine is taken into account by means of variable air gap permeations depending on the position of the machine rotor.

III.2.3 Magnetically Coupled Electric Circuit Method

Any magnetic circuit, whether static (transformer) or dynamic (rotating machine) can be modeled by an equivalent electrical circuit. In this approach, the asynchronous machine is considered to be a set of circuits (R, L) connected electromagnetically. The specific and mutual inductances of the stator and rotor play an important role in this modeling who's their values can be determined in different ways. Moreover, precise knowledge of these inductors will lead to additional information on the signals characterizing the machine, such as currents, voltages and speed. The approach of the multiple coupled electric circuits is based on the Kirchhoff's laws. Thanks to design of a detailed model of an induction machine having m stator circuits and n-rotor bars and if in this method, magnetic saturation is neglected, it is however possible to observe the defects to the rotor and the stator. After having drawn up the equivalent scheme under operation normal conditions, it is possible then to write the equations

of the meshed network and to simulate the faults in the rotor by the breaks of the rotor bars and/or an end-ring segment (S. Hamdani, 2012) (T. Omar, et al,2005)**.**

III.3 Modeling of the IM using Coupled Circuit Method

The first objective of this modeling is to highlight the influence of mechanical faults on the temporal quantities of the asynchronous machine (current, speed, torque ...). Therefore, it is essential to make some assumptions which aim to facilitate the equation of the electrical circuits of the machine. In the used model, we have assumed the linearity of the magnetic circuit. This hypothesis allowed us to use the concept of self-inductance and the mutual inductance between stator and rotor.

III.3.1 Stator

The stator of the machine constitutes a three-phase system. The three phases are modeled by a resistor R_{si} in series with an inductance L_{si}. The machine is connected to a source of balanced voltage which can be the grid or a voltage inverter (Figure III-1).

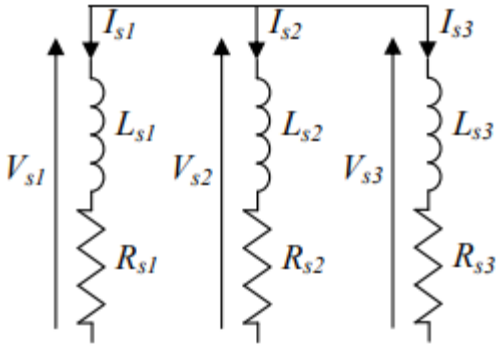

Figure 0.1: Stator electrical circuit

III.3.2 Rotor

The rotor of the asynchronous machine is composed of Nr rotor bars housed in notches. The set of two adjacent bars as well as the ring segments of short circuit that connects them constitute a rotor loop. One of the shorting rings also constitutes an additional loop which makes the number of loops in the rotor cage equal to Nr + 1. Each bar as well as each segment

of the ring is modeled by a resistor in series with an inductor, as shown in the figure bellow (S. Hamdani, et al, 2008)

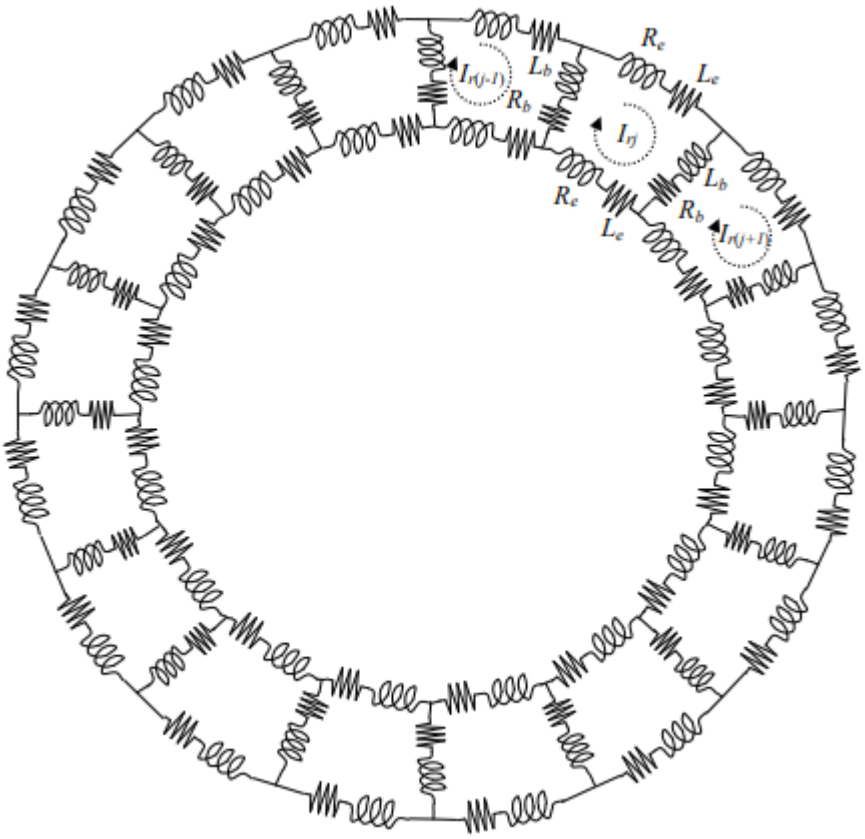

Figure 0.2: Equivalent electrical circuit of the squirrel cage rotor

III.3.3 Equations of the IM

For modeling of the induction machine, few assumptions were taken into consideration; negligible saturation, uniform air gap, the stator windings are sinusoidally distributed and the inter-bar current is also negligible. (T. Omar, et al, 2005):

III.3.3.1 Stator Voltage Equations

The general voltage equation of the stator can be written as

$$[V_s] = [R_s][I_s] + \frac{d[\phi_s]}{dt} \qquad \text{(III-1)}$$

Where

$$[\phi_S] = [L_s][I_s] + [L_{sr}][I_r] \quad \text{(III-2)}$$

Substituting 1 into 2 we have the following:

$$[V_s] = [R_s][I_s] + \frac{d([L_s][I_s])}{dt} + \frac{d([L_{sr}][I_r])}{dt} \quad \text{(III-3)}$$

Where $[L_s]$ is constant, we obtain,

$$[V_s] = [R_s][I_s] + [L_s]\frac{d([I_s])}{dt} + [L_{sr}]\frac{d([I_r])}{dt} + [I_r]\frac{d([L_{sr}])}{dt} \quad \text{(III-4)}$$

and,

$$\frac{d([L_{sr}])}{dt} = \frac{d([L_{sr}])}{d\theta_r}\frac{d\theta_r}{dt} = \frac{d([L_{sr}])}{d\theta_r}\omega_r \quad \text{(III-5)}$$

Then,

$$[V_s] = [R_s][I_s] + [L_s]\frac{d([I_s])}{dt} + [L_{sr}]\frac{d([I_r])}{dt} + [I_r]\frac{d([L_{sr}])}{d\theta_r}\omega_r \quad \text{(III-6)}$$

Since,

$$[V_s] = [V_{as} \quad V_{bs} \quad V_{cs}]^T \quad \text{(III-7)}$$

$$[I_s] = [I_{as} \quad I_{bs} \quad I_{cs}]^T \quad \text{(III-8)}$$

$$[I_r] = [I_{r1} \quad I_{r2} \quad I_{r3} \ldots I_{rnb} \quad I_{re}]^T \quad \text{(III-9)}$$

With,

$[V_s]$: is the terminal stator voltage vector;

$[\phi_s]$: is the stator flux vector;

$[I_s]$: is the stator current vector;

$[I_r]$: is the rotor loop current vector;

$[L_s]$: is symmetric 3x3 matrix represents the stator inductance:

$$[L_s]=\begin{bmatrix} L_{am}+L_{sl} & M_s & M_s \\ M_s & L_{bm}+L_{sl} & M_s \\ M_s & M_s & L_{cm}+L_{sl} \end{bmatrix} \quad \text{(III-10)}$$

$[R_s]$: is symmetric 3x3 matrix represents the stator inductance:

$$[R_s]=\begin{bmatrix} r_s & 0 & 0 \\ 0 & r_s & 0 \\ 0 & 0 & r_s \end{bmatrix} \quad \text{(III-11)}$$

Where r_s is the resistance of the stator winding which depends on material's conductance and the dimension of the windings.

III.3.3.2 Rotor Voltage Equations

Applying Kirchhoff law to the k^{th} mesh we have:

$$2(R_b+R_e)i_j - R_b i_{j+1} - R_b i_{j-1} - R_e i_e + \frac{d}{dt}\begin{bmatrix} (L_{rjrj})+2(L_b+L_e)i_j+(L_{rjrj+1}-I_b)i_{j+1} \\ +(L_{rjrj-1}-I_b)i_{j-1}+\ldots-L_e i_e+L_{rjs1}i_{s1}+\ldots+L_{rjsm} \end{bmatrix} \quad \text{(III-12)}$$

After applying Kirchhoff law to the whole meshes, this leads to:

$$[V_r]=[R_r][I_r]+\frac{d\phi_r}{dt} \quad \text{(III-13)}$$

Where,

$$[\phi_r]=[L_r][I_r]+[L_{rs}][I_s] \quad \text{(III-14)}$$

Then,

$$[V_r] = [R_r][I_r] + \frac{d([L_r][I_r])}{dt} + \frac{d([L_{rs}][I_s])}{dt} \quad \text{(III-15)}$$

Where, $[L_r]$ is constant, the equation (III-15) becomes:

$$[V_r] = [R_r][I_r] + [L_r]\frac{d([I_r])}{dt} + [L_{rs}]\frac{d([I_s])}{dt} + [I_s]\frac{d([L_{rs}])}{dt} \quad \text{(III-16)}$$

With,

$$\frac{d([L_{rs}])}{dt} = \frac{d([L_{rs}])}{d\theta_r}\frac{d\theta_r}{dt} = \frac{d([L_{rs}])}{d\theta_r}\omega_r \quad \text{(III-17)}$$

Accordingly,

$$[V_r] = [R_r][I_r] + [L_r]\frac{d([I_r])}{dt} + [L_{rs}]\frac{d([I_s])}{dt} + [I_s]\frac{d([L_{rs}])}{d\theta_r}\omega_r \quad \text{(III-18)}$$

where,

$$[V_r] = [V_{r1} \quad V_{r2} \quad V_{r3} \ldots V_{rnb} \quad V_{re}]^T \quad \text{(III-19)}$$

and,

$$[\phi_r] = [\phi_{r1} \quad \phi_{r2} \quad \phi_{r3} \ldots \phi_{rnb} \quad \phi_{re}]^T \quad \text{(III-20)}$$

With,

$[V_r]$: is the terminal rotor voltage vector; in case of a cage rotor, the rotor end-ring voltage is $V_{re} = 0$, and the rotor loop voltages are $V_{rk} = 0, (k = 1, 2 \ldots nb)$

$[\phi_r]$: is the rotor flux vector;

$[R_r]$: is a symmetric (nb+1) x (nb+1) matrix represents the rotor resistance:

$$[R_r]=\begin{bmatrix} R_{b0}+R_{b(n_b-1)}+\frac{2R_e}{n_b} & -R_b & \dots & 0 & \dots & \dots & -R_{b(n_b-1)} & :\frac{R_e}{n_b} \\ \dots & \dots & \dots & \dots & \dots & \dots & \dots & :\dots \\ \dots & \dots & \dots & \dots & \dots & \dots & \dots & :\dots \\ 0 & \dots & -R_{b(j-1)} & R_{bj}+R_{b(j-1)}+\frac{2R_e}{n_b} & -R_{bj} & \dots & 0 & :\dots \\ \dots & \dots & \dots & \dots & \dots & \dots & \dots & :\dots \\ \dots & \dots & \dots & \dots & \dots & \dots & \dots & :\dots \\ -R_{b(n_b-1)} & \dots & 0 & \dots & \dots & -R_{b(n_b-1)} & R_{b(n_b-2)}+R_{b(n_b-1)}+\frac{2R_e}{n_b} & :\frac{R_e}{n_b} \\ \dots & \dots & \dots & \dots & \dots & \dots & \dots & :\dots \\ \frac{R_e}{n_b} & \dots & \dots & \dots & \dots & \dots & \frac{2R_e}{n_b} & :R_e \end{bmatrix} \quad \text{(III-21)}$$

Where, R_{bk} and R_e are the resistances of rotor bar and the end ring respectively, similarly to the stator resistance, it depends on the conductance of the material and the dimensions of the rotor loops and the end ring.

$[L_r]$: is a symmetric matrix (nb+1, nb+1) rotor inductance;

$$[L_r]=\begin{bmatrix} L_{am}+2L_b+\frac{2L_e}{n_b} & M_{rr}-L_b & \dots & \dots & M_{rr} & \dots & M_{rr}-L_b & -\frac{L_e}{n_b} \\ \dots & \dots & \dots & \dots & \dots & \dots & \dots & :\dots \\ \dots & \dots & \dots & \dots & \dots & \dots & \dots & :\dots \\ M_{rr}-L_b & \dots & M_{rr}-L_b & L_{am}+2L_b+\frac{2L_e}{n_b} & M_{rr}-L_b & M_{rr} & \dots & :\dots \\ \dots & \dots & \dots & \dots & \dots & \dots & \dots & :\dots \\ \dots & \dots & \dots & \dots & \dots & \dots & \dots & :\dots \\ M_{rr}-L_b & \dots & M_{rr} & \dots & \dots & M_{rr}-L_b & L_{am}+2L_b+\frac{2L_b}{n_b} & :-\frac{L_e}{n_b} \\ \dots & \dots & \dots & \dots & \dots & \dots & \dots & :\dots \\ \frac{-L_e}{n_b} & \dots & \dots & \dots & \dots & \dots & -\frac{L_e}{n_b} & :L_e \end{bmatrix} \quad \text{(III-22)}$$

$[L_{sr}]$: is a $3xn_b$ matrix comprised of the mutual inductances between the stator coil and the rotor loops:

$$\left[L_{sr}\right]=\begin{bmatrix} L_{sr11} & L_{sr12} & \cdots & L_{sr1n_b} & L_{sr1e} \\ L_{sr21} & L_{sr22} & \cdots & L_{sr2n_b} & L_{sr2e} \\ L_{sr31} & L_{sr32} & \cdots & L_{sr3n_b} & L_{sr3e} \end{bmatrix} \tag{III-23}$$

and,

$$\left[L_{sr}\right]=\left[L_{sr}\right]^T \tag{III-24}$$

III.3.3.3 Mechanical Equation

The mechanical equation, which governs the operation of the asynchronous machine, is:

$$J\frac{d\omega_r}{dt}+T_r=T_e \tag{III-25}$$

With,

$$\frac{d\theta_r}{dt}=\omega_r \tag{III-26}$$

The electromagnetic torque can be calculated from the co-energy

$$T_e=\left(\frac{\partial W_{co}}{\partial\theta_r}\right) \tag{III-27}$$

θ_r : is the mechanical angle indicating the rotor position. The co-energy W_{co} can be expressed through:

$$W_{co}=\frac{1}{2}\left[\left[I_s^T\right]\left[L_s\right]\left[I_s\right]+\left[I_s^T\right]\left[L_{sr}\right]\left[I_r\right]+\left[I_r^T\right]\left[L_{rs}\right]\left[I_s\right]+\left[I_r^T\right]\left[L_r\right]\left[I_r\right]\right] \tag{III-28}$$

Then,

$$T_{e_{co}} = \frac{1}{2}\left[\left[I_s^T\right]\left[\frac{\partial L_s}{\partial \theta_r}\right]\left[I_s\right]+\left[I_s^T\right]\left[\frac{\partial L_{sr}}{\partial \theta_r}\right]\left[I_r\right]+\left[I_r^T\right]\left[\frac{\partial L_{rs}}{\partial \theta_r}\right]\left[I_s\right]+\left[I_r^T\right]\left[\frac{\partial L_r}{\partial \theta_r}\right]\left[I_r\right]\right] \qquad \text{(III-29)}$$

For a healthy machine or one with broken bars, the electromagnetic torque is a function of only stator and rotor currents and mutual inductances between the stator and the rotor. Its expression can be given by the below equation according to (A. Ghoggal, et al, 2005):

$$T_{e_{co}} = \frac{1}{2}\left[\left[I_s^T\right]\left[\frac{\partial L_{sr}}{\partial \theta_r}\right]\left[I_r\right]+\left[I_r^T\right]\left[\frac{\partial L_{rs}}{\partial \theta_r}\right]\left[I_s\right]\right] \qquad \text{(III-30)}$$

Since $\left[L_{sr}\right]$ and $\left[L_{rs}\right]$ are equal, then:

$$T_e = \left[I_s^T\right]\left[\frac{\partial L_{sr}}{\partial \theta_r}\right]\left[I_r\right] \qquad \text{(III-31)}$$

III.3.3.4 Total Voltage Equation

$$\begin{bmatrix}[V_s]\\ [V_r]\end{bmatrix} = \begin{bmatrix}[R_s] & [0]\\ [0] & [R_r]\end{bmatrix}\begin{bmatrix}[I_s]\\ [I_r]\end{bmatrix} + \begin{bmatrix}[L_s] & [L_{sr}]\\ [L_{rs}] & [L_r]\end{bmatrix}\frac{d}{dt}\begin{bmatrix}[I_s]\\ [I_r]\end{bmatrix} + \omega_r \frac{d}{d\theta_r}\begin{bmatrix}[L_s] & [L_{sr}]\\ [L_{rs}] & [L_r]\end{bmatrix}\begin{bmatrix}[I_s]\\ [I_r]\end{bmatrix} \qquad \text{(III-32)}$$

III.3.3.5 Total Model Equation

The governing model for both stator and rotor of the IM could be as follows

$$\begin{bmatrix}[V]\\ [T_e - T_r]\\ 0\end{bmatrix} = \begin{bmatrix}[R]+\dfrac{d[L]}{d\theta_r} & [0]\\ [0] & \begin{bmatrix}0 & 0\\ 1 & 0\end{bmatrix}\end{bmatrix}\begin{bmatrix}[I]\\ [\omega_r]\\ \theta_r\end{bmatrix} + \begin{bmatrix}[L] & [0]\\ [0] & \begin{bmatrix}J & 0\\ 1 & 0\end{bmatrix}\end{bmatrix}\frac{d}{dt}\begin{bmatrix}[I]\\ [\omega_r]\\ \theta_r\end{bmatrix} \qquad \text{(III-33)}$$

Hence,

$$\frac{d}{dt}\begin{bmatrix}[I]\\ [\omega_r]\\ \theta_r\end{bmatrix}=\begin{bmatrix}[L] & [0]\\ [0] & \begin{bmatrix}J & 0\\ 1 & 0\end{bmatrix}\end{bmatrix}^{-1}\left(\begin{bmatrix}[V]\\ [T_e-T_r]\\ 0\end{bmatrix}-\begin{bmatrix}[R]+\dfrac{d[L]}{d\theta_r} & [0]\\ [0] & \begin{bmatrix}0 & 0\\ 1 & 0\end{bmatrix}\end{bmatrix}\begin{bmatrix}[I]\\ [\omega_r]\\ \theta_r\end{bmatrix}\right) \qquad \text{(III-34)}$$

III.4 Ball Bearing Modeling

The ball bearing is considered as a spring – damper – mass system, as shown in Figure III-4, with an applied radial load, and considering the radial clearance (is the play between the ball and raceway perpendicular to the bearing axis) between the elements. The outer race is rigidly fixed to the housing, therefore it doesn't rotate, and the inner race is fixed rigidly with the motor shaft are the lumped mass. The rolling elements which transmit the force between inner and outer races are modeled as a damper – contact spring pair, because they are in constant relative motion with the races. Elastic deformation between raceways and rolling elements produces a non-linear phenomenon between force and deformation, which is obtained by the Hertzian theory (A. J. Grajales, et al, 2014)

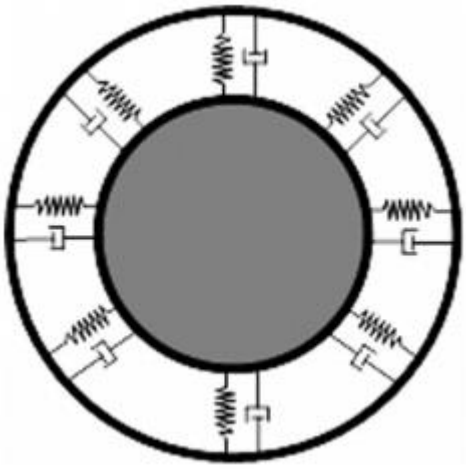

Figure 0.3: Bearing model replaced by spring and dash-pot.

III.4.1 Calculating the Contact Force

Hertzian contact theory is used to calculate the contact force between the ball and the raceway over a long period (F.Kong, et al, 2018). According to the Hertzian contact deformation theory, the non-linear relation load–deformation is given by (M.S. Patil, et al, 2010):

$$F = K\delta_r^n \tag{III-35}$$

Where δ_r is the spring deformation, K is the load – deformation factor or Hertzian elastic contact deformation constant, and n is the load - deformation exponent which is: 3/2 for ball bearings and 10/9 for roller bearings. The load–deflection factor K depends on the contact geometry. The ball and the raceway contact are as shown in Figure III-4,

The load–deflection factor K depends on the contact geometry, Where Total deflection between two raceways is the sum of the approaches between the rolling elements and each raceway. Using this we get:

$$K = \left[\frac{1}{\left(1/K_i\right)^{1/n} + \left(1/K_o\right)^{1/n}} \right]^n \tag{III-36}$$

K_i And K_o inner and outer raceways to ball contact stiffness, respectively, which are obtained using.

$$K_p = 2.15\times10^5 \sum \rho^{-1/2} \left(\delta^*\right)^{-3/2} \tag{III-37}$$

Where, ∑ρ is the curvature sum, which is calculated using the radii of curvature of a couple of principal planes that pass through the point of contact. δ* is the dimensionless contact deformation based on curvature difference (A. J. Grajales, et al, 2014).

To define the radial deflection, a diagram is shown in the below figure (Figure III.4)

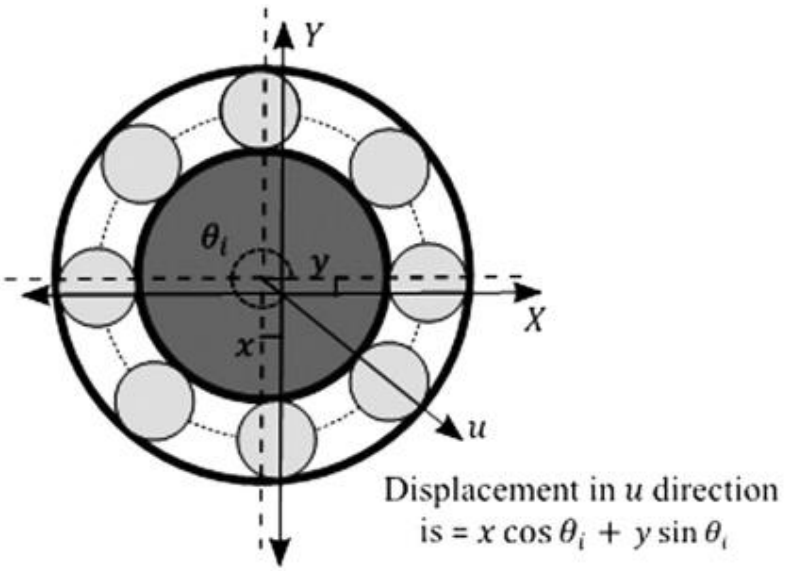

Figure 0.4: Schematic diagram of a ball bearing (A. J. Grajales, et al, 2014)

The radial deflection at the i^{th} ball, at any angle θ_i is given by $\left[\left(x\ cos\theta_i + y\ sin\theta_i\right) - Cr\right]$, where x and y are the deflection along the axis X and Y, and C_r is the internal radial clearance.

Eq (III.35) after Substituting is,

$$F=K\left[\left(x\ cos\theta_i + y\ sin\theta_i\right) - Cr\right]^{3/2} \qquad \text{(III-38)}$$

Given that the Hertzian forces produce only in case of contact deformation, the springs of the model must act only in compression. In addition, the respective spring force comes into play when the instantaneous spring length is shorter than is unstressed length because the term in the bracket should be positive; if not the separation between ball and race takes place and the resulting force is set to zero. The total restoring force is the sum of the restoring forces from each of the rolling elements. Calculating the total restoring force along the X- and Y-axis we obtain: (M.S. Patil, et al, 2010)

$$Fx = \sum_{i=1}^{z} K\left[\left(x\cos\theta_i + y\sin\theta_i\right) - C_r\right]^{3/2}\cos\theta_i \qquad \text{(III-39)}$$

$$Fy = \sum_{i=1}^{z} K\left[\left(x\cos\theta_i + y\sin\theta_i\right) - C_r\right]^{3/2} \sin\theta_i \qquad \text{(III-40)}$$

III.4.2 Model of the Localized Defect

The defect is modeled as a half sinusoidal wave, the total deflection of the paths of bearing is the sum of the characteristic of the defect and that of the static deflection considered. Radial displacement is obtained by considering the resulting distortion, the defect on the outer raceway and inner raceway are show respectively in figure III-5 (a) and (b), (M.S. Patil, et al, 2010).

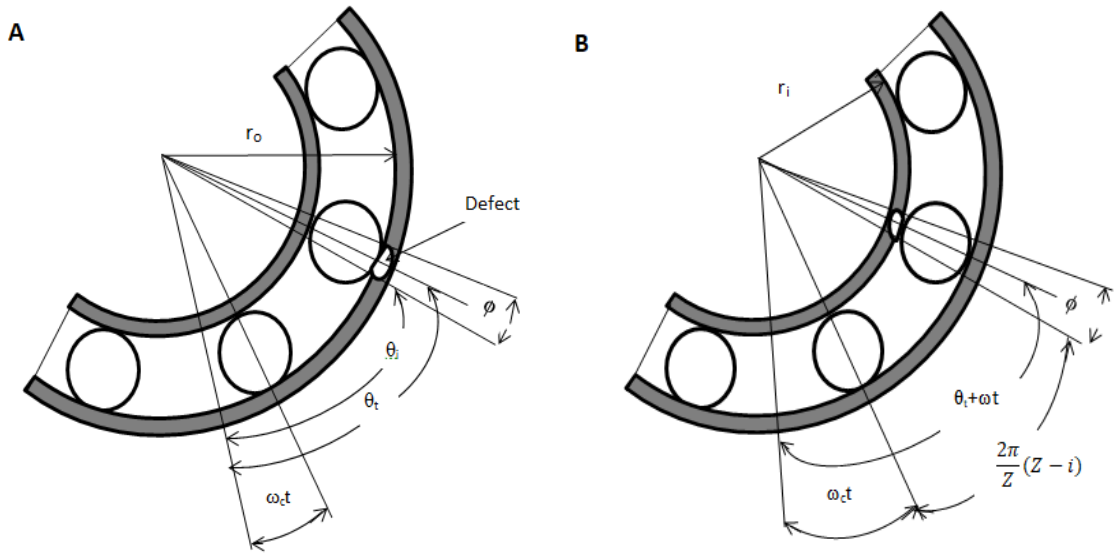

Figure 0.5: (A) Defect on outer race and (B) defect on inner race

The restoring force for the presence of defect on the bearing race is given as:

$$Fx_D = \sum_{i=1}^{z} K\left[\left(x\cos\theta_i + y\sin\theta_i\right) - \left(C_r + H_f\right)\right]^{3/2} \cos\theta_i \qquad \text{(III-41)}$$

$$Fy_D = \sum_{i=1}^{z} K\left[\left(x\cos\theta_i + y\sin\theta_i\right) - \left(C_r + H_f\right)\right]^{3/2} \sin\theta_i \qquad \text{(III-42)}$$

With

$$H_f = H_D \sin \frac{\pi}{\varphi}\left(\theta_t - \theta_i\right) \quad \text{(III-43)}$$

$$\varphi = \frac{Defect\ size}{Raceway\ radius}$$

If the defect is on the outer race

The inner race is moving at the shaft speed (ω) and the ball center at the speed of the cage (ω_c). The ball center is offset from the inner race by an angle of:

$$\theta_t = (\omega_c - \omega)t + 2\pi Z\left(Z - i\right) \quad \text{(III-44)}$$

Where, $i = Z$ to 1

III.4.3. Equation of Motion

Applying Newton's law of motion to the shaft – inner race system in the x and y directions, the equations of motion for a two degree of freedom system are obtained and written as follows:

$$M\ddot{x} + c\dot{x} + F_{XD} = 0 \quad \text{(III-45)}$$

$$M\ddot{y} + c\dot{y} + F_{YD} = W \quad \text{(III-46)}$$

These equations are second order non-linear differential equations; their solution could be fairly obtained by converting them into first order differential equations.

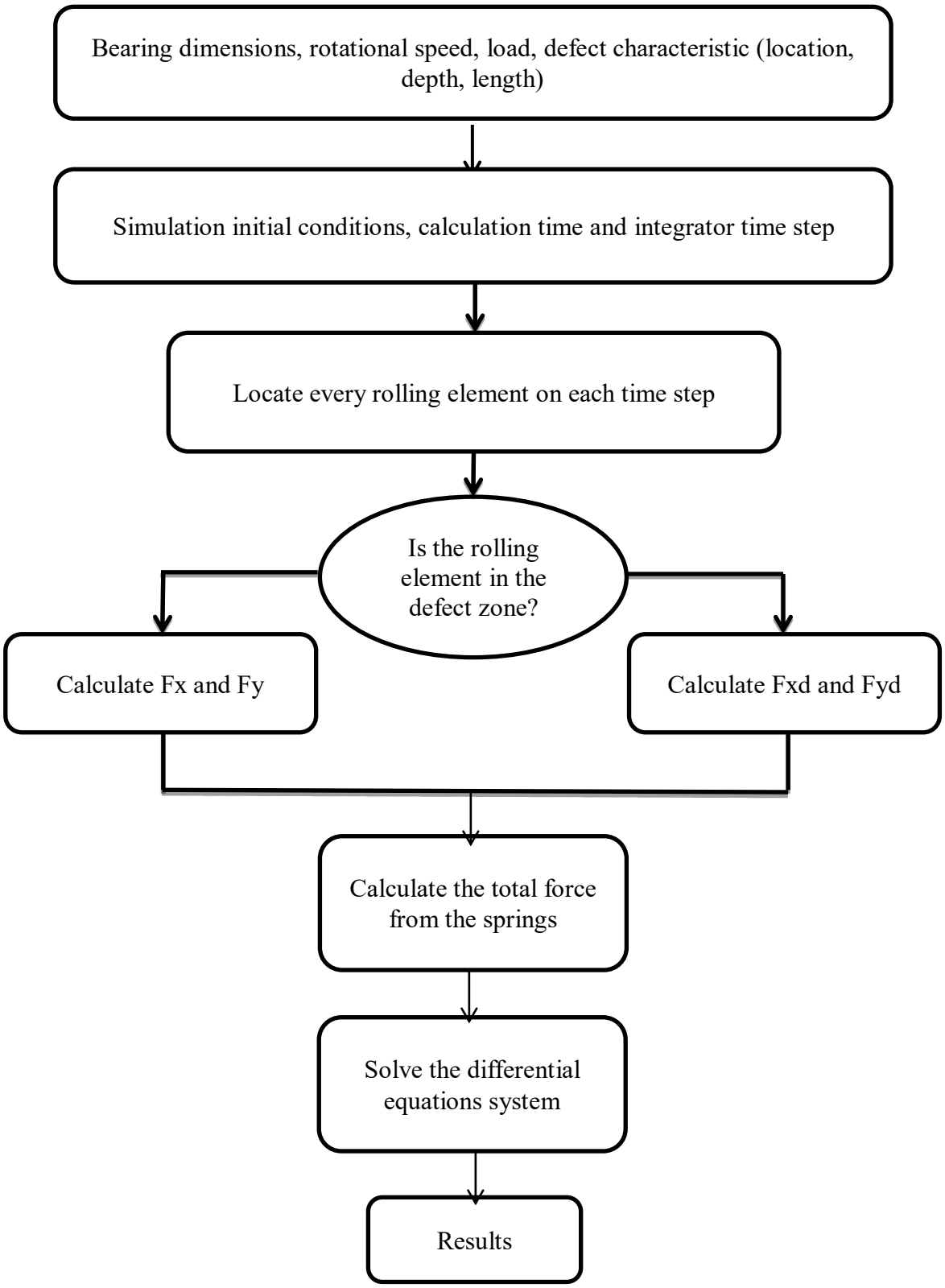
Bearing dimensions, rotational speed, load, defect characteristic (location, depth, length)
Simulation initial conditions, calculation time and integrator time step
Locate every rolling element on each time step
Is the rolling element in the defect zone?
Calculate Fx and Fy
Calculate Fxd and Fyd
Calculate the total force from the springs
Solve the differential equations system
Results

Figure 0.6: Process flow diagram

III.4.4 Transmission of the Fault to the Stator Current

Bearings are members of rigidity and liaison; their defects cause vibrations in the machine. However, the vibrations generated within a bearing are of low amplitude seem to be a random noise. When damage occurs, a pulse occurs whenever the defect is involved in a contact; the mechanical resonance frequencies of the structure are excited and will be modulated by the characteristic fault frequency, therefore the damage depends on the geometry of the bearing and the location of the shelling. The relationship of the bearing vibration to the stator current spectrum can be determined by remembering that any air gap eccentricity produces anomalies in the air gap flux density. In the case of a dynamic eccentricity that varies with rotor position, the oscillation in the air gap length causes variations in the air gap flux density. This, in turn, affects the inductances of the machine producing stator current harmonics. Since ball bearings support the rotor, any bearing defect will produce a radial motion between the rotor and stator of the machine. The mechanical displacement resulting from the damaged bearing causes the air gap of the machine to vary in a manner that can be described by a combination of rotating eccentricities moving in both directions. The effect of a bearing defect depends on its severity and the rotation speed of the machine. The spectral content of the current due to each of the faults will therefore be given by the following expressions (A. Brahim, 2009) (R. Schoen, et al, 1995):

Outer race defect: $$f_{am\_ex} = \left| f_s \pm k f_{ex} \right|$$

Inner race defect: $$f_{am\_in} = \left| f_s \pm f_r \pm k f_{in} \right|$$

Ball defect: $$f_{am\_bi} = \left| f_s \pm f_{cage} \pm k f_{bi} \right|$$

Where f_s is the fundamental frequency of the current signal, f_r is the rotation speed and f_{ex}, f_{in}, f_{bi} and f_{cage} are characteristic frequencies of bearing defects .

In terms of signal processing, it can be noticed that the effect of the fault-related rotor movement on the stator current is an amplitude modulation of the fundamental sine wave, due to the effect of the modified permeance on the fundamental MMF wave (M. Blödt, et al, 2008)

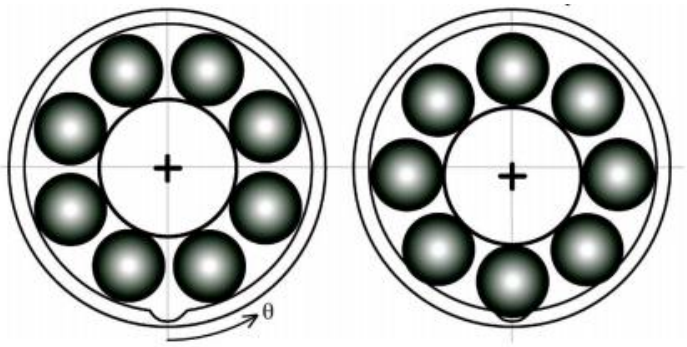

Figure 0.7: Radial rotor movement due to an outer bearing raceway defect

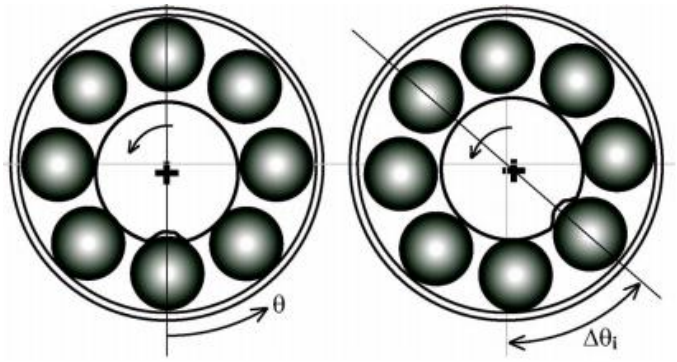

Figure 0.8: Radial rotor movement due to an inner bearing raceway defect

In order to understand the transmission of the rolling defect on the stator current, it is important to study its effect on the magneto-motive forces (MMF).

III.4.4.1 Effect on rotor MMF

When damage occurs, for example a hole in the outer race, each time a ball passes in a hole, a mechanical resistance will appear when the ball tries to leave the hole. The consequence is a small increase of the load torque at each contact between the defect and another bearing element. Under a bearing fault, the load torque as a function of time can be described by a constant component Γ_0 and an additional component varying at the

characteristic frequency f_c. The load torque can therefore be described by: (M. Blödt, et al, 2008)

$$\Gamma_{load}(t) = \Gamma_0 + \Gamma_c \cos(\omega_c t) \tag{III-47}$$

where, Γ_c is the amplitude of the bearing fault-related torque variations, and $\omega_c = 2\pi f_c$.

$$\Gamma_{load}(t) = \Gamma_0 + F_{yd} r_{o,i} \tag{III-48}$$

$$\Gamma_{load}(t) = \Gamma_0 + \sum_{i=1}^{z} K\left[\left(x\cos\theta_i + y\sin\theta_i\right) - \left(C_r + H_f\right)\right]^{3/2} \sin\theta_i . r_{o,i} \tag{III-49}$$

The application of the mechanical equation of the machine leads to the influence of the torque variations on motor speed ω_r, i.e.

$$\sum \Gamma(t) = \Gamma_{motor}(t) - \Gamma_{load}(t) = J \frac{d\omega_r}{dt} \tag{III-50}$$

$$\Leftrightarrow \omega_r(t) = \frac{1}{J} \int_t \left(\Gamma_{motor}(\tau) - \Gamma_{load}(\tau)\right) d\tau \tag{III-51}$$

where Γ_{motor} the electromagnetic torque produced by the machine, and J is the total inertia of the system machine load. In steady-state, the motor torque is assumed to be equal to the constant part of the load torque, i.e. $\Gamma_{motor}(t) = \Gamma_0$

This leads to:

$$\omega_r(t) = -\frac{1}{J}\int_{t_0}^{t} \Gamma_c \cos(\omega_c \tau) d\tau + C = -\frac{\Gamma_c}{J\omega_c} \sin(\omega_c t) + \omega_{r0} \tag{III-52}$$

The mechanical speed consists, therefore, of a constant component ω_{r0} and a sinusoidally varying one.

The next step is the calculation of the mechanical rotor position θ_r, which is the integral of the mechanical speed, i.e.

$$\theta_r(t) = \int_{t_0}^{t} \omega_r(\tau) d\tau = \frac{\Gamma_c}{J\omega_c^2} \cos(\omega_c t) + \omega_{r0} t \qquad \text{(III-53)}$$

The integration constant has been assumed to be equal to zero. In contrast to the healthy machine where $\theta_r(t) = \omega_{r0} t$, variations at the characteristic frequencies are present on the mechanical rotor position.

The variations of the mechanical rotor position θ_r have an influence on the rotor MMF. In a normal state, the rotor MMF in the rotor reference frame R is a wave with p pole pairs and a frequency sf_s and is given by

$$F_r^{(R)}(\theta, t) = F_r \cos(p\theta' - s\omega_s t) \qquad \text{(III-54)}$$

where, θ' is the mechanical angle in the rotor reference frame, and s is the motor slip. The transformation between the rotor and stator reference frames is defined by $\theta = \theta' + \theta_r$. Using (III-54), this leads to

$$\theta' = \theta - \omega_{r0} t - \frac{\Gamma_c}{J\omega_c^2} \cos(\omega_c t) \qquad \text{(III-55)}$$

Thus, the rotor MMF given in (III-55) can be transformed to the stationary stator reference frame using (III-54) and $\omega_{r0} = \omega_s(1-s)/p$, i.e.

$$F_r(\theta, t) = F_{r,1} \cos(p\theta - \omega_s t - m\cos(\omega_c t) + \varphi) \qquad \text{(III-56)}$$

where $m = p\Gamma_c / (J\omega_c^2)$

φ : Phase shift of rotor currents relative to stator currents.

This equation shows that the rotor magneto-motive force rotates at the same speed as the stator FMM and the effect of torque variations appears by phase modulation, characterized by the introduction of the term $m\cos(w_c t)$ in the phase of FMM.

The sum of the two FMM gives us the total magneto-motive force present in the air gap of the machine

$$F_{tot} = F_{s,1}\cos(p\theta - \omega_s t) + F_{r,1}\cos(p\theta - \omega_s t - m\cos(\omega_c t) + \varphi) \quad \text{(III-57)}$$

III.4.4.2 Effect on Flux Density and Stator Current

The air gap flux density B is the product of total MMF and permeance. First, the air gap length and the resulting permeance are assumed constant. The additional fault-related flux density components are obtained by considering the interaction between the modified rotor MMF and the permeance. This leads to

$$B = F_{tot}\mathrm{A} = F_{s,1}\mathrm{A}\cos(p\theta - \omega_s t) + F_{r,1}\mathrm{A}\cos(p\theta - \omega_s t - m\cos(\omega_c t) + \varphi) \quad \text{(III-58)}$$

The fundamental of this wave is therefore a sum of two components: The resulting component of the rotor FMM is phase modulated at the characteristic frequency of the fault f_c, the component of the stator FMM is unchanged. Phase modulation of the FMM therefore translates in the same way to the induction in the air gap.

The magnetic flux is defined by the integral of the magnetic induction B over a surface A

$$\Phi(\mathrm{t}) = \iint_A \vec{B}.d\vec{A} \quad \text{(III-59)}$$

In order to obtain the flux in each phase of the machine, we integrate the induction B according to the length l_m of the machine and the mechanical angle θ in the stator frame. Therefore, taking into account only the fundamentals of flux density, the flux $\Phi(t)$ in an arbitrary coil can be expressed in the general form:

$$\Phi(t) = \Phi_s\cos(\omega_s t) + \Phi_r\cos(\omega_s t + m\cos(\omega_c t) - \phi_r) \quad \text{(III-60)}$$

The induced voltage $V_i(t)$ corresponding to this flux is:

$$V_i(t) = \frac{d\Phi}{dt} = -\omega_s\Phi_s\sin(\omega_s t) - \omega_s\Phi_r\sin(\omega_s t + m\cos(\omega_c t) - \phi_r) \quad \text{(III.61)}$$

$$+m\sin(\omega_c t)\Phi_r \sin(\omega_s t + m\cos(\omega_c t) - \phi_r)$$

We study relatively low torque oscillations. The last term can therefore be neglected in the following. The total induced voltage is the sum of the voltages induced in all the coils of the stator's windings. The resulting signal is also a phase modulated signal with the same modulation index *m*. The voltage in the phases of the stator is imposed by the voltage source; the resulting stator current is linearly related to the induced voltage $V_i(t)$ and has the same frequency. Consequently, the phase-shifted stator current $i_{t0}(t)$ for an arbitrary phase in the presence of an oscillating torque is expressed by:

$$i_{t0}(t) = i_s(t) + i_r(t) = I_s \sin(\omega_s t) + I_r \sin(\omega_s t + m\cos(\omega_c t - \phi_A) - \phi_r) \qquad \text{(III-62)}$$

ϕ_r : is the phase angle of modulation.

This shows that the fundamental component of the current $i_{t0}(t)$ is the sum of two components: The term $i_s(t)$ results from the stator MMF. The term $i_r(t)$, which is a direct consequence of the rotor MMF, shows the phase modulation due to torque and speed induced oscillations.

III.5 Total Dynamic Equation of the Bearing

The solution to equations (III.63) and (III.64) is obtained by converting these into first order differential equations using state space variable method.

$$M\ddot{x} + c\dot{x} + F_{XD} = 0 \qquad \text{(III-63)}$$

$$M\ddot{y} + c\dot{y} + F_{YD} = W \qquad \text{(III-64)}$$

III.5.1 Bearing without defect

By replacing the expressions of F_{XD} and F_{YD} in the equations (62) and (63) we obtain:

$$M\ddot{x} + c\dot{x} + \sum_{i=1}^{n} K\left[(x\cos(\theta_i) + y\sin(\theta_i) - Cr)\right]^{(3/2)} \cos(\theta_i) = 0 \qquad \text{(III-65)}$$

$$M\ddot{y} + c\dot{y} + \sum_{i=1}^{n} K\left[(x\cos(\theta_i) + y\sin(\theta_i) - Cr)\right]^{(3/2)} \sin(\theta_i) = W \qquad \text{(III-66)}$$

State space representation of equations (III-67) and (III-68):

$$\begin{bmatrix} M & 0 \\ 0 & M \end{bmatrix}\begin{bmatrix} \ddot{x} \\ \ddot{y} \end{bmatrix} + \begin{bmatrix} c & 0 \\ 0 & c \end{bmatrix}\begin{bmatrix} \dot{x} \\ \dot{y} \end{bmatrix} + \begin{bmatrix} \sum_{i=1}^{n} K\left[(x\cos(\theta_i) + y\sin(\theta_i) - Cr)\right]^{(3/2)} \cos(\theta_i) \\ \sum_{i=1}^{n} K\left[(x\cos(\theta_i) + y\sin(\theta_i) - Cr)\right]^{(3/2)} \sin(\theta_i) \end{bmatrix} = \begin{bmatrix} 0 \\ W \end{bmatrix} \qquad \text{(III-67)}$$

A computer program is developed to obtain the solution and plot the results.

To solve these differential equations, we have to reduce it into two first order differential equations. This step is taken because MATLAB uses a Runge-Kutta method to solve differential equations, which is valid only for first order equations.

Let

$$\begin{aligned} x &= z(1) \\ \dot{x} &= z(2) \\ y &= z(3) \\ \dot{y} &= z(4) \end{aligned} \qquad \text{(III-68)}$$

$$\dot{z}(1) = z(2) \qquad \text{(III-69)}$$

$$\dot{z}(2) = -\frac{c}{m} z(2) - \sum_{i=1}^{n} \left(\frac{K}{m}\right)\left((z(1)\cos(\theta_i) + z(3)\sin(\theta_i) - Cr)^{(3/2)} \cos(\theta_i)\right) \qquad \text{(III-70)}$$

$$\dot{z}(3) = y(4) \qquad \text{(III-71)}$$

$$\dot{z}(4) = -\frac{c}{m} z(4) - \frac{w}{m} - \sum_{i=1}^{n} (\frac{K}{m})((z(1)cos(\theta_i) + z(3)sin(\theta_i) - Cr)^{(3/2)} sin(\theta_i)) \quad \text{(III-72)}$$

III.5.2 Bearing with defect

The state space representation of ball bearing with defect is as follow:

$$\begin{bmatrix} M & 0 \\ 0 & M \end{bmatrix} \begin{bmatrix} \ddot{x} \\ \ddot{y} \end{bmatrix} + \begin{bmatrix} c & 0 \\ 0 & c \end{bmatrix} \begin{bmatrix} \dot{x} \\ \dot{y} \end{bmatrix} + \begin{bmatrix} \sum_{i=1}^{n} K\left[(xcos(\theta_i) + ysin(\theta_i)) - (Cr - H_f) \right]^{(3/2)} cos(\theta_i) \\ \sum_{i=1}^{n} K\left[(xcos(\theta_i) + ysin(\theta_i)) - (Cr - H_f) \right]^{(3/2)} \sin(\theta_i) \end{bmatrix} = \begin{bmatrix} 0 \\ W \end{bmatrix} \quad \text{(III-73)}$$

The solution of these differential equations is accomplished as for the model without defect using MATLAB, with:

$$\dot{z}(1) = z(2) \quad \text{(III-74)}$$

$$\dot{z}(2) = -\frac{c}{m} z(2) - \sum_{i=1}^{n} (\frac{K}{m})((z(1)cos(\theta_i) + z(3)sin(\theta_i) - (Cr - H_f))^{(3/2)} cos(\theta_i)) \quad \text{(III-75)}$$

$$\dot{z}(3) = y(4) \quad \text{(III-76)}$$

$$\dot{z}(4) = -\frac{c}{m} z(4) - \frac{w}{m} - \sum_{i=1}^{n} (\frac{K}{m})((z(1)cos(\theta_i) + z(3)sin(\theta_i) - (Cr - H_f))^{(3/2)} sin(\theta_i)) \quad \text{(III-77)}$$

III.6 Summary

In this chapter, we have presented the modeling part of asynchronous squirrel cage machine as well as the modeling of ball bearing. This machine model made it possible to understand the physical phenomena involved in the appearance of bearing defects on the torque and stator current. Moreover, a MATLAB program is developed to solve the differential equations and simulate the defect on the raceways.

CHAPTER IV

TIME DOMAIN SIMULATION RESULTS

IV.1 Introduction

In this chapter, time-domain simulation is presented for healthy induction machine and faulty ball bearing with the influence of ball bearing faults on induction machine torque, rotor speed and stator current. The main parameters of the machine were simulated including the torque, speed and the stator currents. Moreover, the parameter of the ball bearing simulated were the displacement, the generated forces in both x and y directions.

IV.2 Simulation results

In this section, a summary of the simulation results for an induction motor model and ball bearing model are presented. The results contain: stator currents; electromagnetic torque; rotor speed and the displacement of ball's bearing, total springs forces and acceleration of balls for X and Y direction.

The simulation is done in healthy and faulty cases of induction machine and ball bearing (defect in outer and inner races).

IV.2.1 Healthy case

In this section, during healthy operations, the motor is at t=0.7s loaded with 2.5N.m, as shown in the figures below. These latter represent the stator currents, the stator voltage, the electromagnetic torque and the rotor speed.

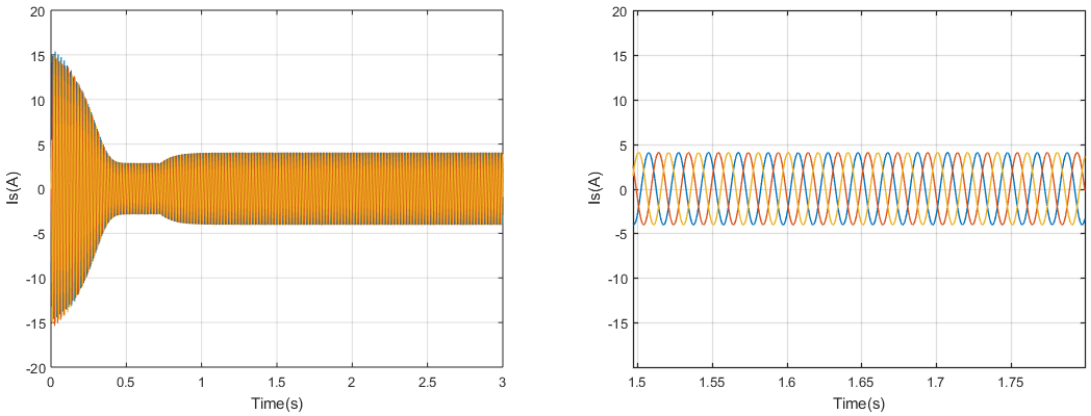

Figure IV. 1: Stator currents of phases a, b and c for healthy operation.

It appears an intense current in transient mode which lasts 0.4s and reaches 15A which is equal to about 5 times the nominal current (2.8A), these are the starting currents to overcome the inertia of the rotor, it represents one of the major problems of the asynchronous machine. When a load is introduced at t=0.7A the current increases until reached 4A.

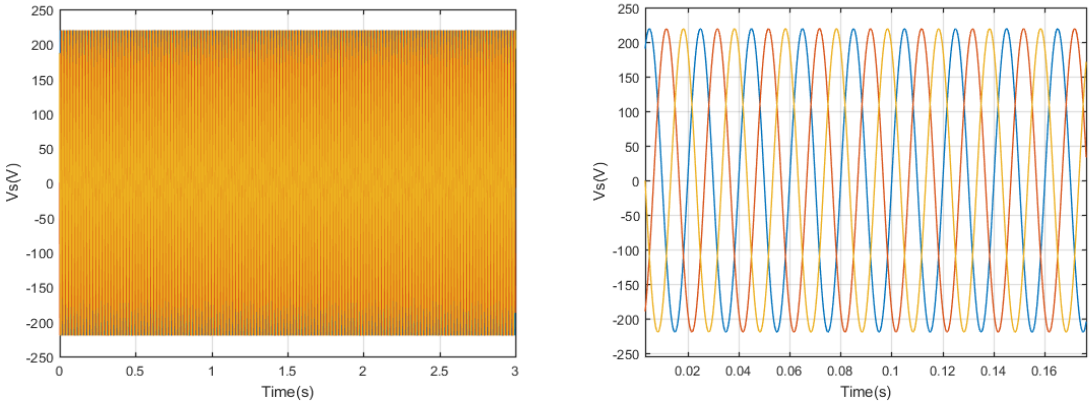

Figure IV. 2: Stator voltage of phases a, b and c for healthy operation.

Figure 0.2 illustrates the three phases of the motor supply voltage which have amplitude of 220V and they are phase-shifted by 120°.

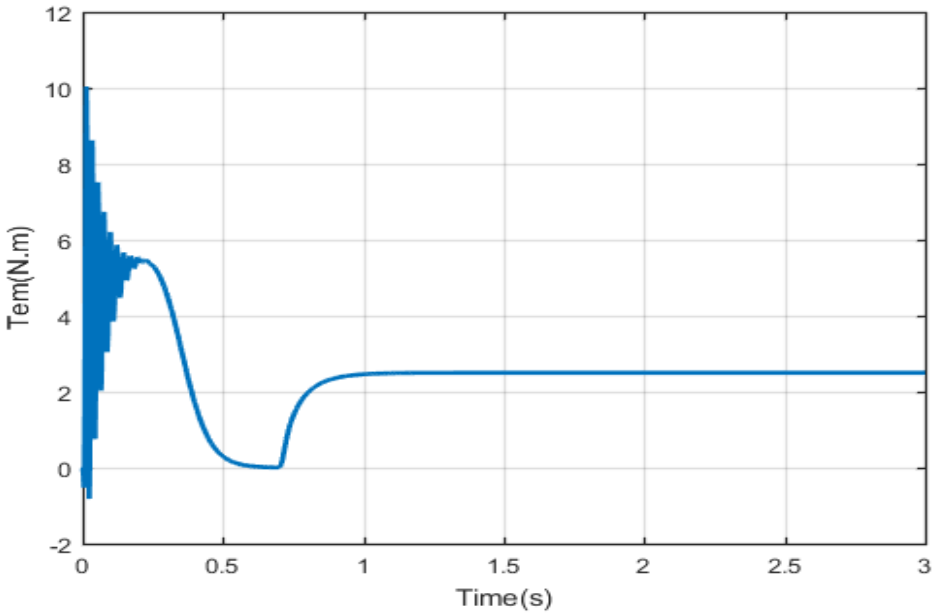

Figure IV. 3: Electromagnetic Torque for healthy operation

Figure 0.3 represents the electromagnetic torque of the motor which makes damped oscillations during the transient regime, these oscillations stabilize at t=0.7s taking a constant value equal to 2.5 N.m.

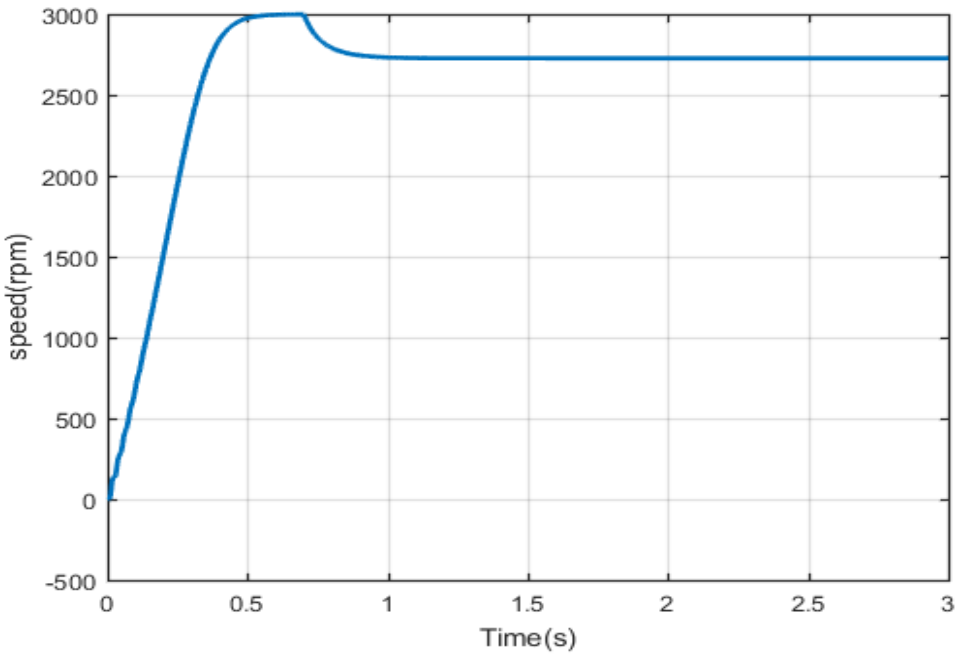

Figure IV. 4: Rotor Speed for healthy operation.

Figure 0.4 shows that the rotor speed with no load steady state condition increases up to 3000 rpm then it deceases at t=0.6s when a mechanical load is injected to obtain as a final value 2750rpm.

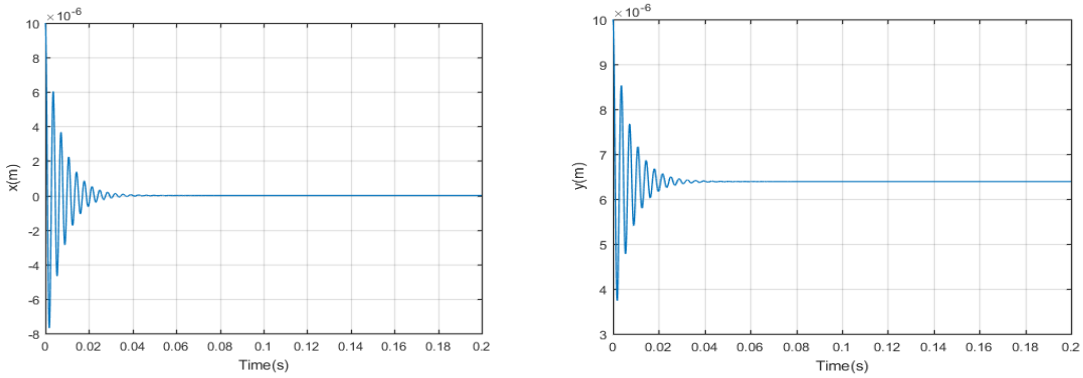

Figure IV. 5: X and Y Direction displacement of balls.

Figure 0.1 and figure illustrate the displacement of balls along X and Y. The displacement is oscillatory with a peak of 10^{-5}m during the transient event for the two figures, this oscillation damped out to take a constant value 0 for x displacement and $6.39x10^{-6}$m for y displacement at 0.06s. We notice that the balls in healthy state make a radial displacement with negligible value.

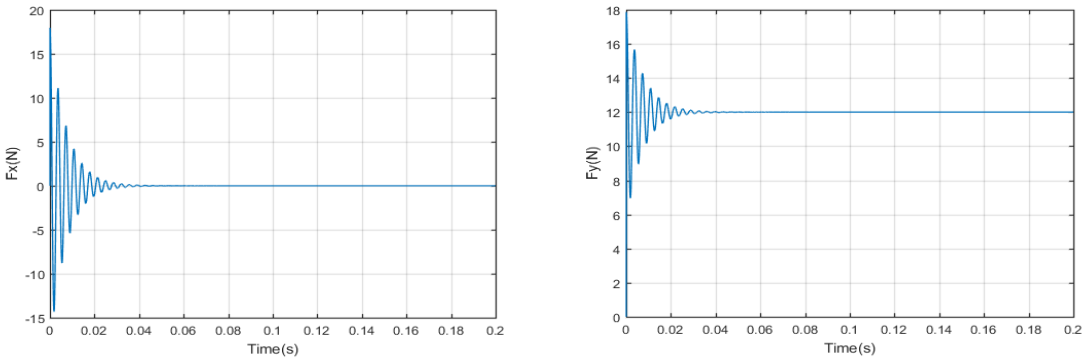

Figure IV. 6: X and Y Direction total spring's forces.

Figure IV.6 illustrate the total springs forces along X and Y, these latter oscillate during the transient event with a peak of 17N for X-Direction forces and 18N for Y-Direction forces. This oscillation damped out to take a constant value 0.N along x axis and about 12N along y axis at 0.06s due to the radial load imposed on y axis.

IV.2.2 Faulty case

In this section, the simulation results of faulty ball bearing are shown, then the effect of bearing defects on the operation of the machine and its influence on the mechanical and electrical quantities, (torque, speed and current).

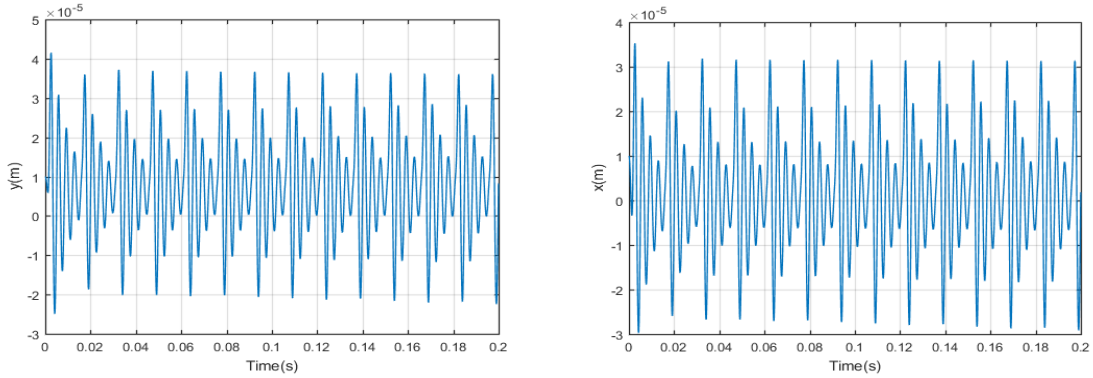

Figure IV. 7: X and Y Direction displacement of balls (with defect).

It is obvious that the figures IV.7 of balls bearing displacement along x and y directions shows the vibration behavior when the ball passes over the defect(on the outer or inner races), because a mechanical resistance will appear when the ball tries to leave the defect, these vibrations are oscillatory, where the amplitude increase during transient event with a peak about $3.5x10^{-5}$ m and $4x10^{-5}$ m for x-displacement and y-displacement respectively and a peak during steady state about $3x10^{-5}$ m and $3.5x10^{-5}$ m for x-displacement and y-displacement respectively (maximum of the amplitude occurs when the defect exist). As the ball moves away from the defect zone, the amplitude decreases and damped to 0 for x-displacement and $6x10^{-6}$m for y-displacement. Due to the rotational movement of the bearing these vibrations are periodic and repeat themselves regularly and lead to a series of impulse.

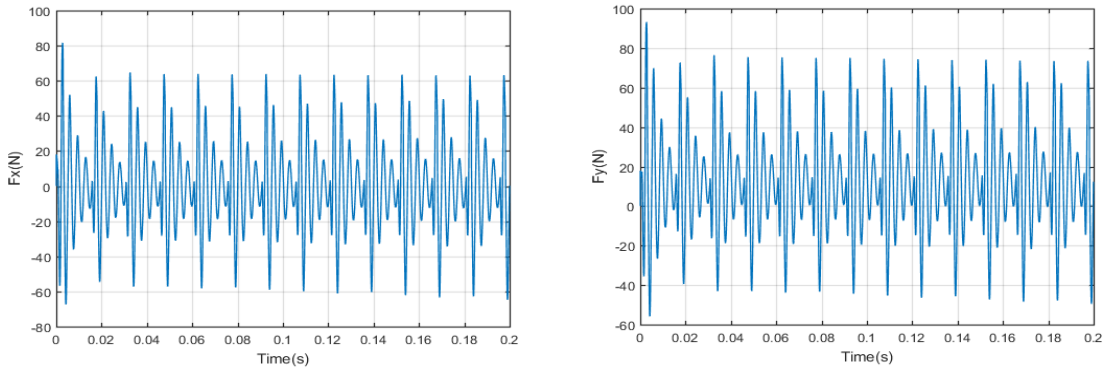

Figure IV. 8: X and Y Direction total spring's forces (with defect).

Figures IV.8 illustrate the total springs forces along x and y directions, it shows the vibrations behavior when the ball passes over the defect on the bearing, these vibrations oscillatory increase with a peak about 60N and 75N during steady state (maximum of the amplitude occurs when the defect exist), then damped when the ball leaves away from the defect. Due to the rotational movement of the bearing these vibrations are periodic and repeat themselves regularly and lead to a series of impulses.

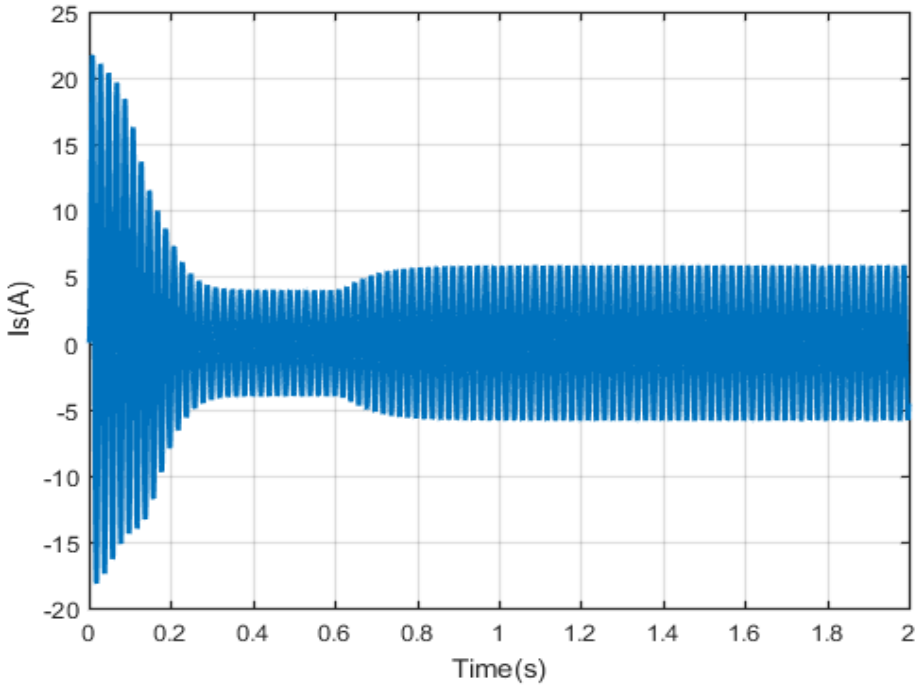

Figure IV. 9: Stator current with bearing fault (inner and outer races defects)

It is difficult to notice the changes in the stator current in the time domain because the fault in the ball bearing in (outer or inner races) is relatively small. Therefore, analyzing its spectrum might give more insight on the faults.

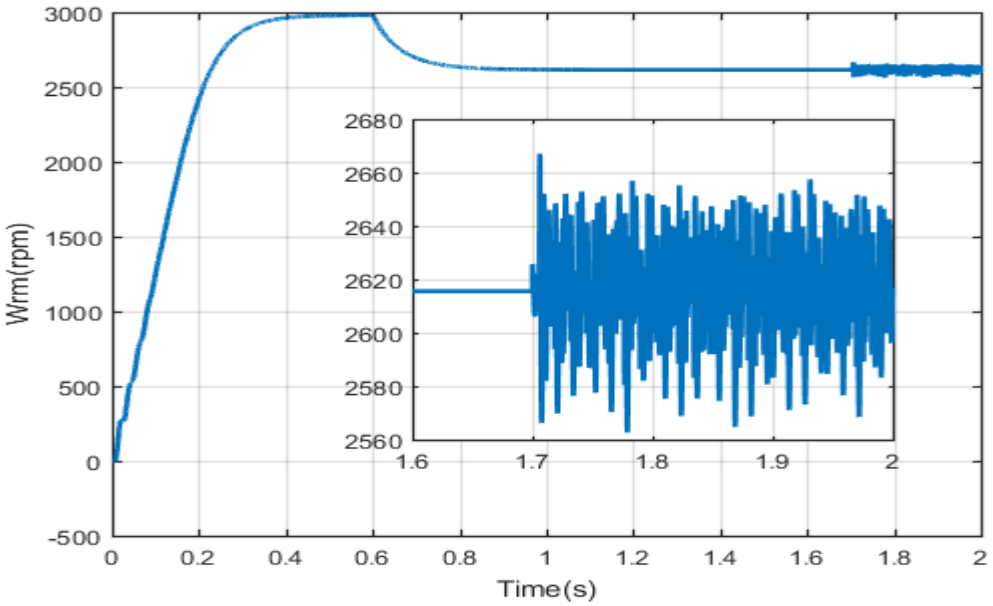

Figure IV. 10: Rotor speed for faulty operation (inner and outer races defects)

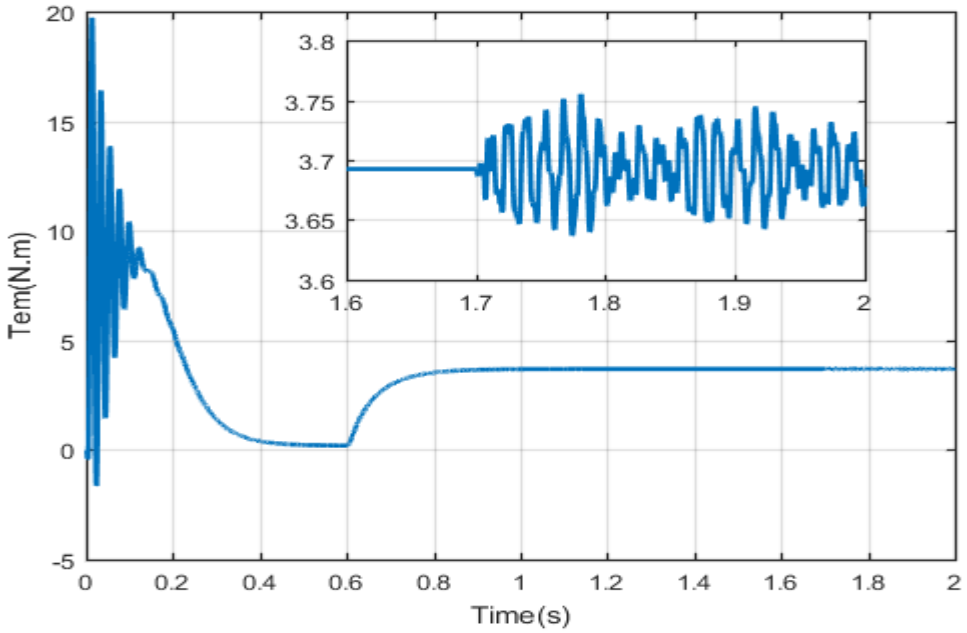

Figure IV. 11: Electromagnetic torque for faulty operation (inner and outer races defects).

Figure IV.10 and IV.11 illustrate the rotor speed and the electromagnetic torque of the machine operating in the presence of a ball bearing fault (in inner race and outer race), When fault occur at 1.7s, it appears a periodic oscillations which damped when the ball moves away from the defect on the rotor speed because the shaft being carried by the faulty bearing, the same thing for the load torque , that's because during the rotation of faulted bearing, shocks are produced causing vibration also torque surges. The periodic repetition of these torque surges over time includes oscillations in the electromagnetic torque of the machine (the fault appears as a non-linear additional load).

IV.3 Summary

In this chapter, simulation results were presented for both induction motor model and ball bearing model in healthy and faulty cases. It is clear that in the presence of localized defect in the raceways (inner or outer) periodic impacts are generated when the balls pass upon these defect which in turn introduce oscillations in the mechanical quantities of the machine, torque and speed.

CHAPTER V

SPECTRAL ANALYSIS RESULTS

V.1 Introduction

Spectral analysis is a technique widely used in diagnosing the faults diagnosis in electrical machines. The fault being reflected by the appearance of additional components and/or the increase in the amplitude of certain components in the spectrum of the stator current, of the instantaneous electric power or the voltage induced after disconnection of the machine from its power supply. In this study, FFT is used on the stator's current, the electromagnetic torque and the rotor speed for the detection of ball bearing fault that shows abnormal frequencies related to these faults in the frequency spectrum.

V.2 Fast Fourier Transform

FFT helps in converting the time domain in frequency domain which reduce the complexity of large transforms, and reduce the computing time, which make it used in signal processing. FFT is widely used in the domain of fault diagnosis of electrical machines.

V.2.1 Spectral Analysis Results Based on FFT

In this section, a summary of the simulation results for the spectral analysis applied for the stator current, electromagnetic torque and rotor speed are presented. The Fast Fourier Transform algorithm is used to perform the spectral analysis which shows frequency continent in the signals.

V.2.1.1 Spectral analysis Results of Healthy IM

Figure V.1 illustrate the spectral analysis of the stator current for a healthy motor, it looks smooth with just the fundamental frequency 50 Hz and very low amplitude sideband frequencies which are maybe due to asymmetries in motor construction caused by elasticity and shaft misalignment.

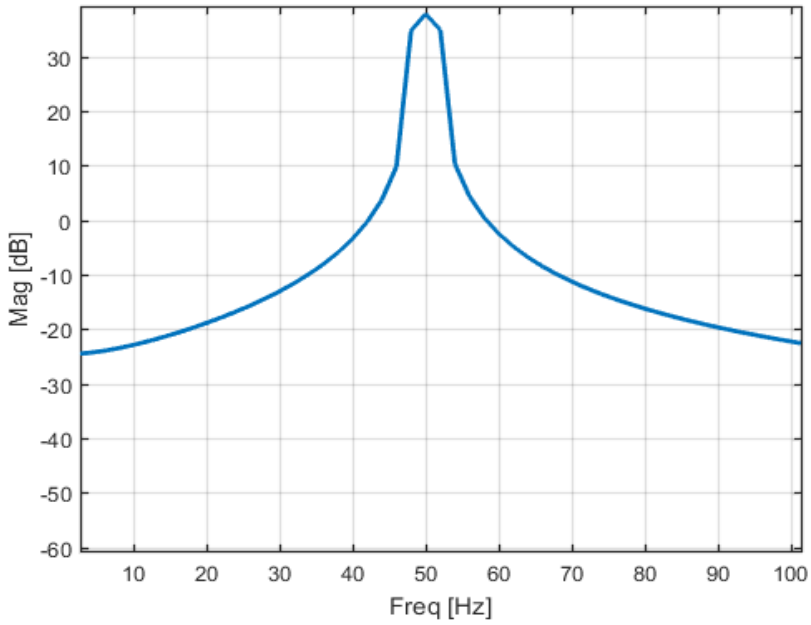

Figure V. 1: Stator Current Spectrum (healthy case)

Figure V.2 and V.3 illustrate the spectral analysis of electromagnetic torque and rotor speed respectively; the figures reveal smooth with no abnormal frequencies appear neither in rotor speed spectrum nor torque spectrum.

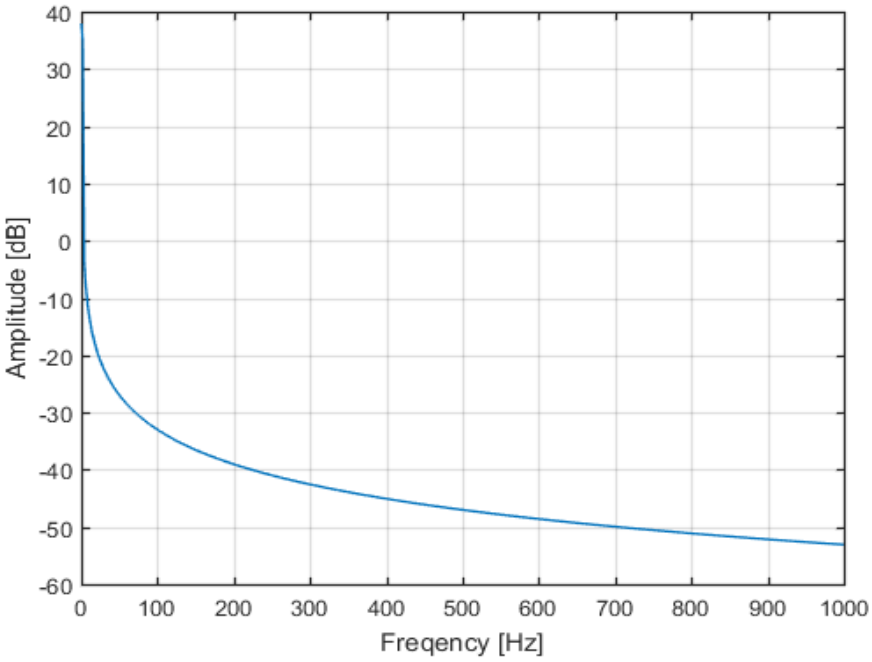

Figure V. 2: Electromagnetic Torque Spectrum (healthy case)

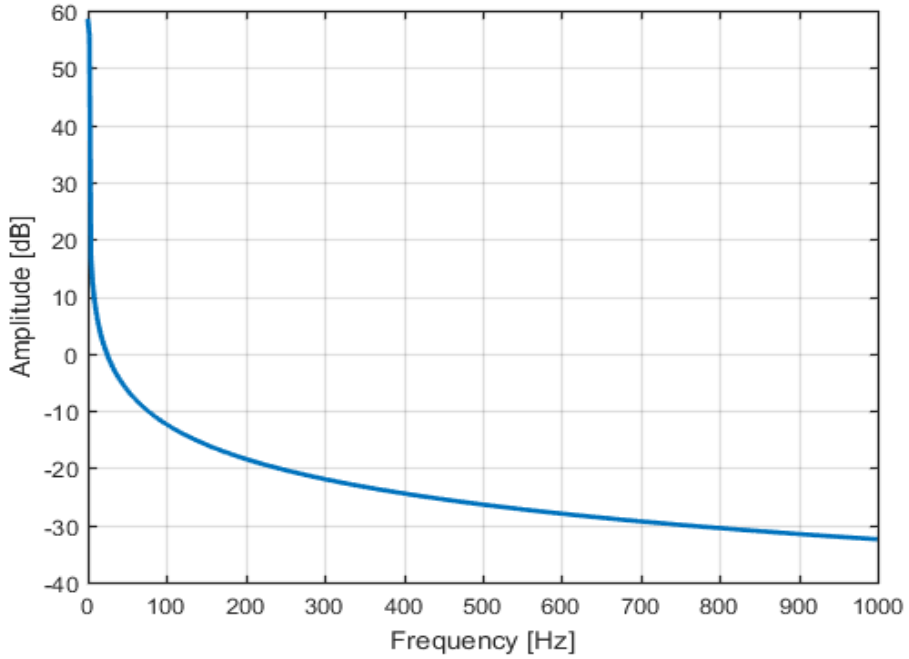

Figure V. 3: Rotor Speed Spectrum (healthy case)

V.2.1.2 Spectral Analysis results of the Induction Motor with Faulty Ball Bearing

The inner and outer races have the same thickness gives a pitch diameter equal to 43.385 mm (PD = 43.385 mm). The bearing has nine balls (n = 9) with an approximated diameter of 11.274 mm (BD = 11.274 mm). Assuming a contact angle, β, of zero degrees and motor operation at the rated shaft speed of fr= 43.6 Hz, the characteristic frequencies of inner raceway and outer raceways are respectively f_i = 235.4 Hz and f_o = 156,9 Hz.

V.2.1.2.1 Inner Race Defect

When bearing defect occur in the inner raceway, radial motion between the rotor and stator of the machine produced. The mechanical displacement resulting from the damaged bearing at bearing fault characteristic frequencies in the inner race f_i causes the air gap of the machine to vary in a manner that can be described by a combination of rotating eccentricities moving in both directions. This motion generates additional frequencies in stator currents which is given by $f_{bf}=|f_s \pm f_r \pm k f_i|$, Where f_s is the electrical stator supply frequency 50 Hz, and k=1, 2, 3…

Table V.1 bellow show approximately the additional frequencies due to inner raceway defect.

Table V.1. Predictable frequencies in stator current for inner raceway defect

Frequency	Full load
f_r	43.6 Hz
f_i	235.4 Hz
f_{bf} (k=1)	329 Hz
f_{bf} (k=2)	564.4 Hz
f_{bf} (k=3)	799.8 Hz

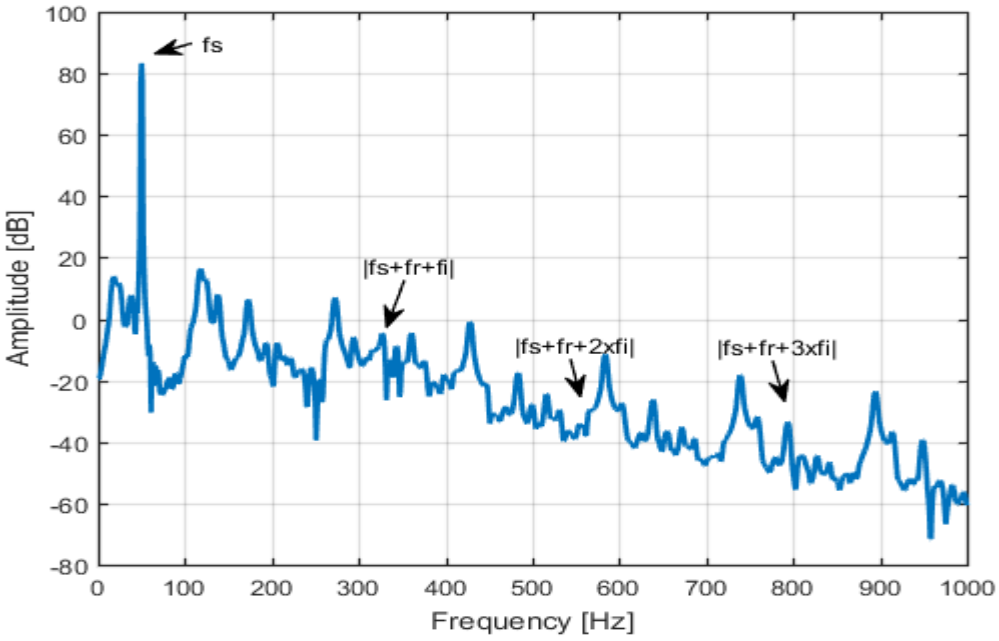

Figure V. 4: Spectral analysis of the stator current with inner raceway defect

Figure V.4 illustrates the stator current spectrum with inner raceway defect, comparing with healthy case, a change of the stator current spectrum where harmonics appears in the current spectrum. The current spectrum shows a characteristic component which corresponds to the frequency combination $|f_s+ f_r+ f_i|$, $|f_s+ f_r+2xf_i|$ and $|f_s+ f_r+3xf_i|$ around stator current, ,where the calculated predictable frequencies in Table 5.1 appear in the figure. This validates the proposed theoretical approach which corresponds to the apparition of the frequencies

combination of the characteristic frequencies of the inner raceway defect and the electrical stator supply frequency $|f_s \pm f_r \pm kxf_i|$ in the current spectrum in the case of inner race defect. In addition, other components appear with increase in the amplitude but they have no direct link to the predicted frequency combination, they may due to an asymmetry in the distribution of the air gap of the motor and the load torque.

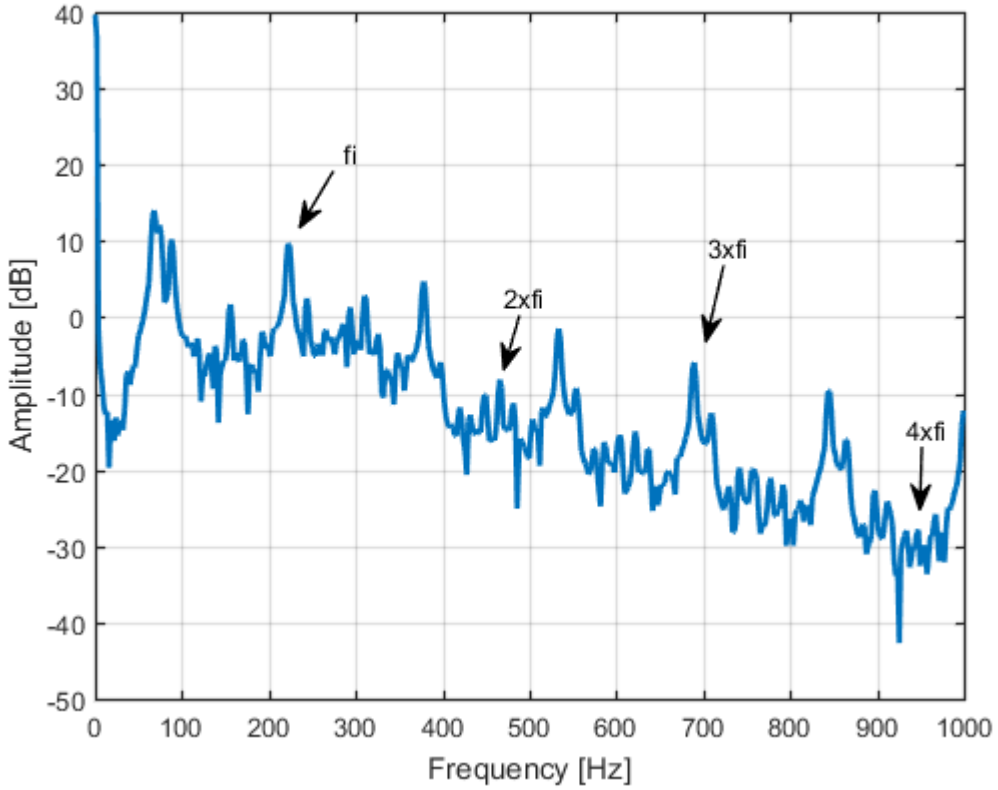

Figure V. 5: Spectral analysis of the electromagnetic torque with inner raceway defect

Figure V.5 illustrate spectral analysis of the electromagnetic torque, comparing with the healthy case, harmonics appear include the characteristic frequencies of the inner raceway defect f_i and its multiples. The characteristic fault frequency f_i clearly appears on the torque spectrum with amplitude of +10 dB, this validates the proposed theoretical approach, which assumes torque variations at the characteristic frequency as a consequence of the bearing fault. Higher harmonics of f_i can be observed in the figure. In addition, other frequencies appear in the torque spectrum but they have no direct link to a predicted characteristic frequency may due to load torque and to an asymmetry in the distribution of the air gap of the motor.

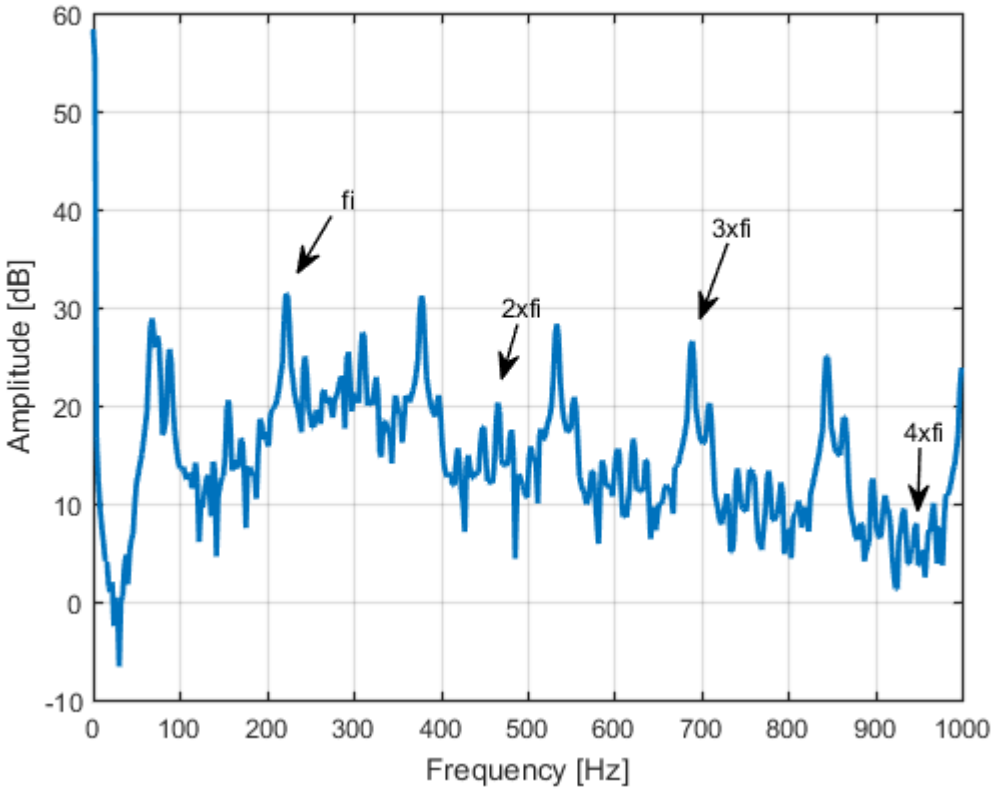

Figure V. 6: Spectral analysis of the rotor speed with inner raceway defect

Figure V.6 illustrate the spectral analysis of rotor speed, comparing with the healthy case, harmonics appear include the characteristic fault frequency of the bearing f_i and its multiples. Higher harmonics of f_i can be observed in the figure with an amplitude of +31dB.

V.2.1.2.2 Outer Race Defect

When outer raceway defect occurs, produce a radial motion between the rotor and stator of the machine. The mechanical displacement resulting from the damaged bearing at bearing fault characteristic frequencies in the outer race f_o causes the air gap of the machine to vary in a manner that can be described by a combination of rotating eccentricities moving in both directions, This motion generates additional frequencies in stator currents which is given by $f_{bf}=|f_s \pm k f_o|$, Where f_s is the electrical stator supply frequency 50 Hz, and k=1,2,3…

Table V.2. Predictable frequencies in stator current for inner raceway defect

Frequency	At Full load
f_r	43.6 Hz
f_o	156.9Hz
f_{bf} (k=1)	206.9Hz
f_{bf} (k=2)	363.8Hz
f_{bf} (k=3)	520.7Hz
f_{bf} (k=4)	677.6 Hz

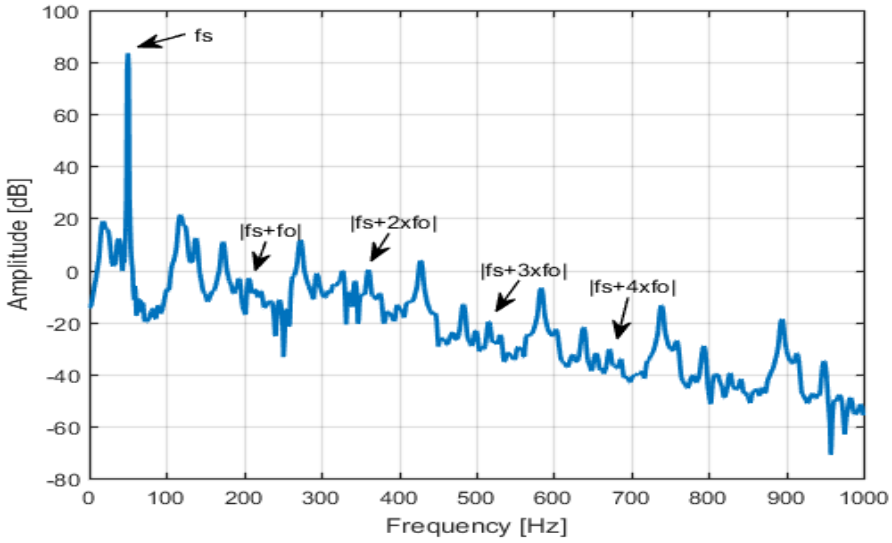

Figure V. 7: Spectral analysis of the stator current with outer raceway defect

Figure V.7 illustrate the stator current spectrum with outer raceway defect, comparing with healthy case, a change of the stator current spectrum where harmonics appears in the current spectrum. The current spectrum shows a characteristics components which corresponds to the frequency combination $|f_s \pm f_o|$,$|f_s \pm 2xf_o|$,$|f_s \pm 3xf_o|$ and $|f_s \pm 4xf_o|$ around stator current, where

the calculated predictable frequencies in Table 5.2 appear in the figure this validates the proposed theoretical approach which correspond to the apparition of frequencies combination of the characteristic frequencies of the outer raceway defect and the electrical stator supply frequency $|f_s \pm kxf_o|$ in the current spectrum in the case of outer race defect. In addition, others components appear with increase in the amplitude but they have no direct link to the predicted frequency combination, they may due to an asymmetry in the distribution of the air gap of the motor and the load torque.

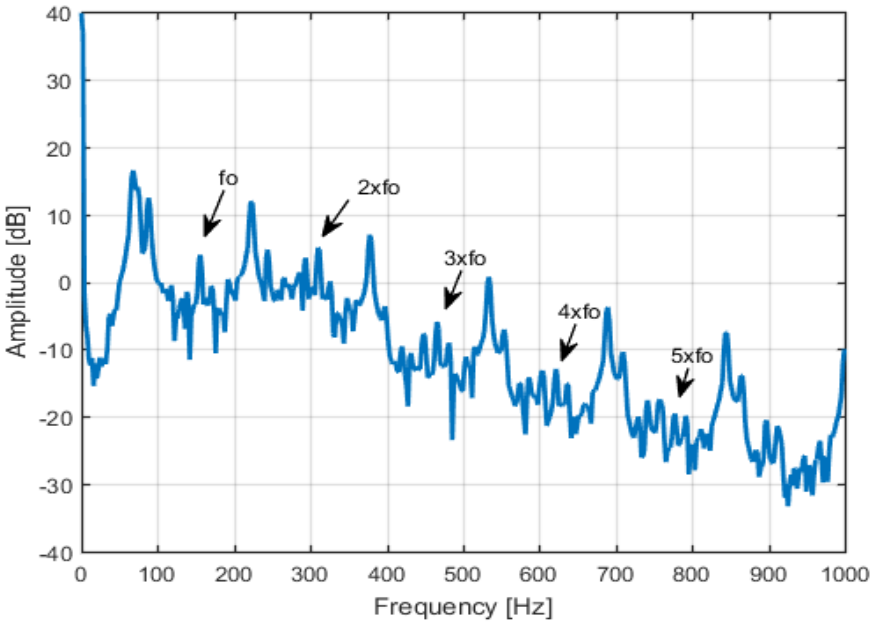

Figure V. 8: Spectral analysis of the electromagnetic torque with outer raceway defect

Figure V.8 illustrate spectral analysis of the electromagnetic torque, as in the case of inner race defect, comparing with the healthy case, harmonics appear include the characteristic frequencies of the outer raceway defect f_o and its multiples. The characteristic fault frequency f_o clearly appears on the torque spectrum with amplitude of +4 dB, this validates the proposed theoretical approach, which assumes torque variations at the characteristic frequency as a consequence of the bearing fault. In addition, other frequencies appear in the torque spectrum but they have no direct link to a predicted characteristic frequency may due to load torque and to an asymmetry in the distribution of the air gap of the motor.

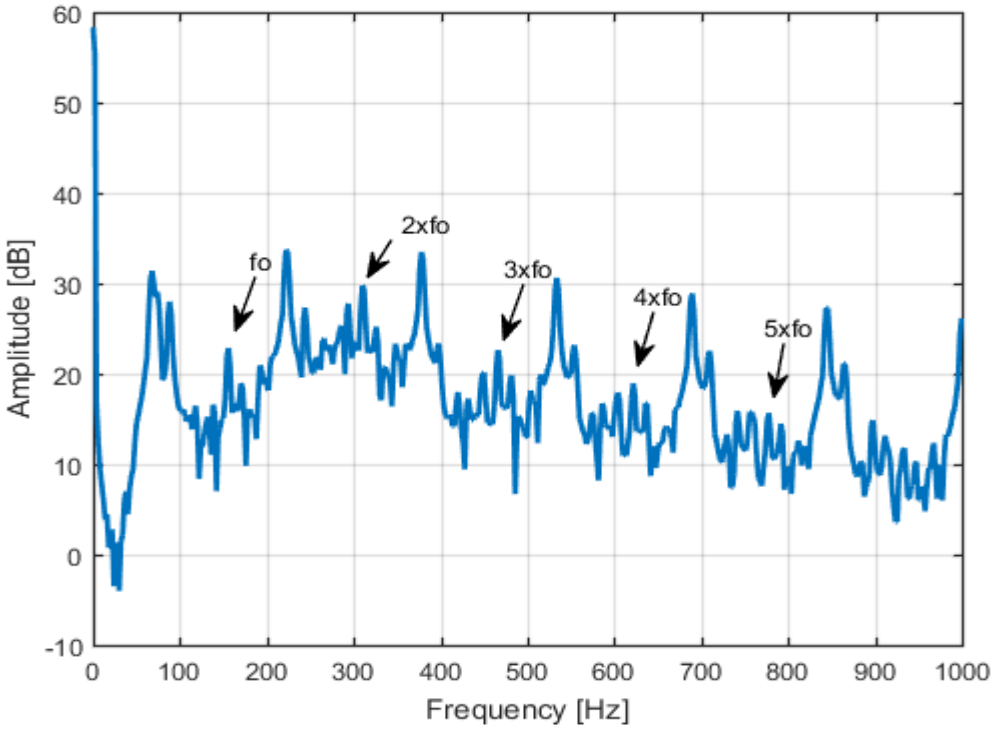

Figure V. 9 : Spectral analysis of the rotor speed with outer raceway defect

Figure V.9 illustrate the spectral analysis of rotor speed, comparing with the healthy case, harmonics appear include the characteristic frequencies of the outer raceway defect f_o and its multiples. The characteristic frequencies of the outer raceway defect f_o appear with amplitude of +22.86dB and its multiples $2xf_o$ is the component with the larges with an amplitude of +30dB.

V.3 Summary

In this chapter the results of spectral analysis based on Fast Fourier Transform are presented which applied in healthy and faulty cases to the induction machine signals current, speed and electromagnetic torque. The spectral analysis shows that characteristic vibration frequencies caused by inner race and outer race faults are visible in the speed and torque spectrum. The torque oscillations lead to changes in the stator current spectrum. The variation in the current spectrum caused by inner race and outer race faults with apparition of

characteristics components allows detection of the defect. Thus the results prove the efficiency of stator current analysis for detecting ball bearing faults by reveal abnormal frequencies with different amplitudes in faulty machine compared with a healthy machine in the same conditions.

CHAPTER VI

CONCLUSION AND RECOMMENDATION FOR FUTURE WORK

Asynchronous machine based electric drive are widely used in industrial applications due to their low coast, performance and ruggedness. However, degraded operating modes may appear during the life the machine. The main reason for machine failures remains ball bearing defects. This work deals with the detection of mechanical failures and more precisely ball bearing failures using a spectrum of a single phase of the stator current of an induction motor.

In this thesis, modeling of asynchronous squirrel cage machine based on coupled magnetic circuit method is presented as well as a model of ball bearing which are simulated in MATLAB software in order to visualize the behavior of the machine when faults occur in ball bearing raceways, inner raceway and outer raceway. Both models are simulated in both healthy and faulty cases to understand the effect of ball bearing failures on the induction machine.

To detect the letters faults, a diagnosis based signal processing method was used, which is the fast Fourier Transform (FFT) that shows the frequency component of machine's signals. Thus any abnormal frequencies appear in the signal are usually related to a certain type of faults for the present dissertation combination of the characteristics frequencies of the inner raceway and outer raceway defects reveals in the stator current spectrum.

During this study it has been shown that in the event of fault oscillations on the speed and the torque appears which are present in frequency domain by harmonics relating to the frequencies characteristics of the ball bearing. Whereas Speed or torque variation due to ball bearing fault influence the stator current spectrum, and as the rolling element bearing support the rotor, defective rolling element bearing generate eccentricity in the air gap with mechanical variations. The air gap eccentricities cause variations in the air gap flux density that produces these variations generate noticeable changes in the stator current spectrum.

The general conclusion of this study is that current signature analysis based on FFT can effectively detect the ball bearing faults in the induction motor.

In the perspectives related to this work, we suggest continuing this study by analyzing others signals such as bearing vibration signal and temperature as well using advanced techniques of diagnosis such as time-frequency techniques and artificial intelligence in which they are more efficient and give more details about the bearing faults.

REFERENCES

A. Glowacz, ” Fault diagnosis of single-phase induction motor based on acoustic signals,” Mechanical Systems and Signal Processing,vol.117, pp. 65-80,2019.

A .H. Bonnett. G.C. Soukup ,”Cause and analysis of stator and rotor failures in three phase squirrel-cage induction motors, ”IEEE Transactions on Industry Applications, VOL. 28, NO.4 :921-937,JULY, 1992.

A. Ibrahim, “Contribution au diagnostic de machines Électromécaniques : Exploitation des signaux Électriques et de la vitesse instantanée,” Thèse de Doctorat, Université de Saint Etienne, 2009.

A.H.Bonnett.” Root cause ac motor failure analysis with a focus on shaft failures “.IEEE Transactions on industry Application, Vol.36, No.5 pp. 435-1448, Septembre/Otober 2000.

B.Vaseghi,”Contribution à l’étude des machines électrique en présences de défaut entre spires Modélisation-Réduction du courant de défaut,” Thèse de doctorat, institut national polytechnique de Lorraine, 2009.

A. Bouzida,” Diagnostic de Défauts des Machines Asynchrones par la Technique du Traitement du Signal,” Thèse de Doctorat, Ecole Nationale Polytechnique (ENP), 2015.

B. Bianchini, F. Immovilli, M. Cocconcelli, R. Rubini, A. Bellini,” Fault Detection of Linear Bearings in Brushless AC Linear Motors by Vibration Analysis,” IEEE Transactions Industrial Electronics, Vol. 58, No. 5, May 2011.

A. CHAOUCH,” Contribution à la modélisation de la machine asynchrone en vue de diagnostic des défauts par analyse spectrale des grandeurs électriques,” Thèse doctorat, Université des sciences et de la technologie d’Oran Mohamed Boudiaf, 2013.

F.Kong, W. Huang, Y.Jiang, W. Wang, X.Zhao, “ A Vibration Model of Ball Bearings with a Localized Defect Based on the Hertzian Contact Stress Distribution,” Shock and Vibration, pp.1–14,2018

G. Didier,”Modélisation et diagnostic de la machine asybchrone en présence de défaillances,” Thèse de Doctorat,l’Université Henri Poincaré, Nancy-I,2004.

G.Y.MASSALA MBOYI,” Analyse vibratoire et estimation de la durrée de vie residuelle des composants mécaniques de guidage en rotation,” Mémoire de fin de cycle ingénieur de l’Université des Sciences et Techniques de Masuku, 2018.

Ghoggal, A., Sahraoui, M., Aboubou, A., Zouzou, S. E., & Razik, H. (n.d.). An Improved Model of the Induction Machine Dedicated to Faults Detection - Extension of the Modified Winding Function. IEEE International Conference on Industrial Technology, 2005.

J. A. Grajales, J. F. López, H. F. Quintero,” Ball bearing vibrations model: Development and experimental validation,” Ingeniería y Competitividad, Volumen 16, No. 2, pp. 279 – 288, 2014.

A. J. Bazurto, E. C. Quispe, R. C. Mendoza,” Causes and Failures Classification of Industrial Electric Motor,” Universidad Autónoma, Occidente, 2016.

J. Cusido, I. Roura, JLR. Martine,"Transient analysis and motor fault detection using the wavelet transform,"MCIA, 2014.

J. Faiz , B. M. Ebrahimi, M. B. B. Sharifian ," Different Faults and Their Diagnosis Techniques in Three-Phase Squirrel-Cage Induction Motors—A Review," Electromagnetics, Vol.26, No.7, pp.543-569. 23 Nov 2006

J. S. Hsu," Monitoring of defects in induction motors through air-gap torque observation," IEEE Transactions on Industry Applications, Vol.31, No.5, pp.1016 -1021, 1995.

J. Penman, H.G. Sedding, B.A. Lloyd, W.T. Fink, «Detection and location of interturn short circuits in the stator windings of operating motors,"IEEE Trasactions on Energy Conversion, Vol.9,No.4,pp.652-658,December,1994.

M. Sahraoui , A. Ghoggal, S.E. Zouzou, M.E. Benbouzid," Dynamic eccentricity in squirrel cage induction motors – Simulation and analytical study of its spectral signatures on stator currents," Simulation Modelling Practice and Theory 16, pp. 1503-1513,2008.

M.Blödt, P. Granjon, B. Raison, G. Rostaing," Models for Bearing Damage Detection in Induction Motors Using Stator Current Monitoring," IEEE Transactions on Industrial Electronics, Vol. 55, No. 4, April 2008.

M.E.H. Benbouzid, M. Vieira, C. Theys," Induction Motors' Faults Detection and Localization Using Stator Current Advanced Signal Processing Techniques," IEEE Transaction on Power Electronics, Vol. 14, No. 1, January 1999.

M.E.K. Oumaamar," Surveillance et diagnostic des des défauts rotoriques et mécaniques de la machine asynchrone avec alimentation équilibrée ou déséquilibrée," Thèse de Doctorat, l'Université de Lorraine, 2012

M.S. Patil, J. Mathew,P.K. Rajendrakumar, S. Desai," A theoretical model to predict the effect of the localized defect on vibrations associated with ball bearing," International Journal of Mechanical Sciences, Vol. 52, No.9, pp.1193-1201, 2010.

A. Mahyob, P. Reghem, G. Barakat," Permeance Network Modeling of the Stator Winding Faults in Electrical Machines," IEEE TRANSACTIONS ON MAGNETICS, VOL. 45, No. 3, MARCH 2009.

N. MEHALA," Condition monitoring and fault diagnosis of induction motor using motor current signature analysis," thesis of doctorate, National institute of technology, KURUKSHETRA, October, 2010.

N. Saad, M. Irfan, R.Ibrahim," Condition Monitoring and Faults Diagnosis of Induction Motors:Electrical Signature Analysis," Taylor & Francis Group,2019.

N. Tandon, A. Choudhury," A review of vibration and acoustic measurement methods for the detection of defects in rolling element bearings," Tribology International 32 ,pp.469-480,1999.

O. Touhami, L.Noureddine , R. Ibtiouen , M.Fadel ," Modeling of the Induction Machine for the Diagnosis of Rotor Defects. Part. I: An Approach of Magnetically Coupled Multiple Circuits," IEEE,pp. 1580-1587,2005.

P. S.Bhowmik , S. Pradhan, M. Prakash," Fault diagnosis and monitoring methods of induction motor: A Review," International Journal of Applied Control, Electrical and Electronics Engineering (IJACEEE) Vol.1, No 1,May 2013

P.J. Tavner, B.G. Gaydon, D.M. Ward, Monitoring generators and large motors, IEE PROCEEDINGS, Vol. 133, Pt. B, No. 3, MAY 1986

R. R. Schoen, T. G. Habetler, F. Kamran, R. G. Bartheld," Motor bearing damage detection using stator current monitoring ," IEEE Transaction on industry applications, Vol. 31, NO 6,1274-1279, November/December 1995.

S. Hamdani,"modélisation, détection et classification des défauts rotoriques de la machine asynchrone à cage," Thèse de Doctorat, Ecole Nationale Polytechnique (ENP), 2012.

S. Nandi, H. A. Toliyat, L. Xiaodong,"Condition monitoring and fault diagnosis of electrical motors-a review,"IEEE Transactions On.Energy Convers., vol. 20,No. 4,pp. 719-729, December 2005.

S.Belhamdi," Diagnostic des défauts de la machine asynchrone contrôlée par différents techniques de commande ," Thèse de doctorat Université de Biskra, Mai, 2014

S.Karmakar, S.Chattopadhyay, M. Mitra, S.Sengupta," Induction Motor Fault Diagnosis: Approach through Current Signature Analysis," Springer Science,2016.

S.KASS," Diagnostic Vibratoire Autonome des Roulements," Thèse de Doctorat Université de Lyon, 2019.

A. Siddique, G.S.Yadava, B.Singh,"A review of stator fault monitoring techniques of induction motors", IEEE Transactionon Energy Conversion, Vol. 20, No. 1, MARCH, 2005.

T.A. Harris, M.N.Kotzalas,Essentiel concepts of bearing technology,5th edition, Taylor & Francis ,2006.

H.A. Toliyat, S. Nandi," Condition monitoring and fault diagnosis of electrical machines— A review," Proc. IEEE-IAS Annual Meeting, Phoenix, AZ,pp. 197-204,1999.

W. Zaabi, Y. Bensalem, H. Trabelsi," Fault Analysis of Induction Machine using Finite Element Method (FEM)," 15th international conference on Sciences and Techniques of Automatic control & computer engineering - STA'2014, Hammamet, Tunisia, December 21-23, 2014.

X. L. Y. Liao, H. A. Toliyat, A. E. Antably and T. A. Lipo, " Multiple coupled circuit modeling of induction machines," IEEE Trans. Ind. Appl, Vol. 31, No.2, pp. 311-317, Mar/Apr 1995.

YE. Zhongming, WU. Bin," A Review on induction Motor Online Fault Diagnosis," Ryerson Polytechnic University, pp.1353-1358.

APPENDICES

Table A.1: Selected Induction Machine and ball bearing Parameters.

Notation	**Definition**	**Unit**
R =63.29 x 10^{-3}	Mean diameter of the machine	m
l = 65 x 10^{-3}	Length of the slots in the stator	m
g = 0.3 x 10^{-3}	Air gap between the stator and the rotor	m
Nr=16	Number of the bars in the squirrel cage rotor	
Ns=90	Number of turns in the stator winding	
Rs =7.828	Single phase winding resistance	Ω
Re=72 x 10^{-6}	End ring resistance	Ω
Le = 0.03 x 10^{-6}	End ring leakage inductance	H
Lb = 0.1 x 10^{-6}	Rotor bar's leakage inductance	H
Lls =28 x 10^{-3}	Stator leakage inductance in each phase	H
K0= 0	Friction coefficient	
J=6 x 10^{-3}	Moment of Inertia	Kg.m2
M=0.6	the mass of the shaft	Kg
K=8.37x10^{7}	Load deflection factor	N/$m^{3/2}$
nb=9	Number of rollers	
n=1.5	Raised power	
Cr = 11.285x10^{-6}	Radial Clearance	m
Ir_Dia= 32.1x10^{-3}	Inner race diameter	m
Or_Dia=54.67x10^{-3}	Outer race diameter	m
α=0	Contact angle	deg
Nss=2800	Shaft speed	Rad/s
d = 11.274x10^{-3}	Ball Diameter	m
D = 43.385x10^{-3}	Pich Diameter	m
C=200	damping factor	N s/m